Journal of Sound and Vibration (2001) **248**(5), 925–953
doi:10.1006/jsvi.2001.3852, available online at http://www.idealibrary.com on IDEAL®

VIBRATION TRANSMISSION THROUGH AN ISOLATOR MODELLED BY CONTINUOUS SYSTEM THEORY

S. KIM AND R. SINGH

Acoustics and Dynamics Laboratory, Department of Mechanical Engineering and The Center for Automotive Research, The Ohio State University, Columbus, OH 43210-1107, *U.S.A.*
E-mail: singh.3@osu.edu

(*Received* 19 *February* 2001, *and in final form* 15 *June* 2001)

This article focuses on the flexural motion of an elastomeric isolator but the longitudinal motion is also considered. The continuous system theory is used to describe mobility or stiffness characteristics and power-based vibration isolation measures. The scope of this study is limited to the frequency domain analysis of a linear time-invariant (LTI) system with a single isolator that is placed between a rigid body and a finite or infinite beam receiver. The upper limit of the frequency range is 4 kHz. Two types of solutions to the Timoshenko beam for a rubber material are critically examined, and the Timoshenko and Euler beam solutions are compared for vibration power measures. Our analysis shows that the shear deformation and rotary inertia must be considered in order to properly describe a thick isolator that effectively transmits flexural motions at higher frequencies. The shear deformation effect is, however, found to be more pronounced as evaluated by the power-based vibration isolation measures at higher frequencies. Further, the roles of isolator parameters such as the static stiffness ratios, shape factors and material properties are investigated. The continuous system theory clearly accounts for the cross-axis coupling terms and it may be further utilized for optimizing vibration isolation schemes over a wide range of frequencies.

1. INTRODUCTION

Vibration isolators are often characterized as discrete elastic elements, with or without viscous or hysteritic damping [1–4]. The compressional stiffness term is typically used to develop isolation system models [2–4] though the transverse (shear) and rotational components are also sometimes specified or included [5–7]. Additionally, at higher frequencies, inertial or standing wave effects occur within the isolator [8, 9]. Nonetheless, the isolators are still modelled by many researchers in terms of spectrally invariant discrete stiffness elements without any cross-axis coupling terms [5–7]. Such descriptions are clearly inadequate at higher frequencies. Consequently, one must adopt the distributed parameter approach. It is the main focus of this article.

Only a few articles have examined the elastomeric devices using the continuous vibration system theories [10–15]. For example, the longitudinal stiffness of an isolator has been described by the wave equation to characterize the material property of an isolator [13]. Also, rubber-like material has been modelled using the wave closure relationship [14]. The Euler beam theory has been adopted to describe the flexural motions of a mount for an active vibration control system [10, 11] and to characterize an isolator [12]. However, no prior article has examined the shear deformation and rotary inertia effects of an isolator. Further, the influence of component parameters on the behavior of an isolation system has

0022-460X/01/500925 + 29 $35.00/0

been investigated using a standing wave description in the longitudinal direction and a static stiffness term in the flexural direction [14]. Yet, the frequency-dependent characteristics of an isolator have not been considered in the previous isolation studies. This article proposes to overcome this particular void in the literature.

2. PROBLEM FORMULATION

Vibration transmitted via multi-dimensional motions of an isolator is conceptually shown in Figure 1 in the context of source, path (isolator) and receiver. A rigid body is employed for the source and the receiver is modelled using two alternate formulations: an infinite beam and then a finite beam with fixed boundary conditions. The analysis focuses on the flexural motion of the isolator but the longitudinal motion is also considered. Though both are assumed to be uncoupled within the isolator, coupling will arise because of the receiver dynamics. Harmonic force and moment excitations are applied at the mass center of source. The scope of this study is strictly limited to the frequency domain analysis of a linear time-invariant (LTI) system with a single isolator that is placed between a rigid body and flexible receiver. Complicating effects such as isolator pre-load, temperature dependence and the like are not considered. Primary objectives of this study are as follows. (1) Develop the frequency response characteristics (mobility or stiffness) of an isolator based on the continuous system theory that includes Timoshenko beam (in the transverse x direction) and the longitudinal (y) wave equation formulation. In particular, critically examine the two types of solutions to the Timoshenko beam for a cylindrical rubber material. (2) Compare the Timoshenko and Euler beam solutions for the effects of shear deformation and rotary inertia of an isolator on vibration power attenuation measures. (3) Investigate the role of isolator parameters such as the static stiffness ratios, shape factors and material properties on isolation measures over a broad range of frequencies.

3. FLEXURAL MODEL OF ISOLATOR USING TIMOSHENKO BEAM THEORY

3.1. MOBILITIES OF A FINITE TIMOSHENKO BEAM

The classical Timoshenko beam theory that describes the effects of shear deformation and rotary inertia has been well studied by many researchers [4, 16–18]. The literature shows that there are two types of solution and two modal functions that exist at high frequencies [4, 16]. However, the high-frequency solution has been ignored by many since this phenomenon has been believed to occur only at extremely high frequencies [4]. Only a few studies have been conducted to examine the dispersion and spectrum relations of the Timoshenko beam structure at high frequencies [17, 18]. In our study, we examine this issue and the harmonic response of an elastomeric beam with free boundary conditions. It is assumed that the shear modulus (G) is very low, which is true for a rubber-like material. Further, the characteristic mobilities are obtained for a semi-infinite beam. The governing equation for an unforced and undamped Timoshenko beam (in flexure) is expressed as follows where E is the Young's modulus, I_S is the area moment of inertia, S is the section area, ρ is the mass density and κ is the shear constant [4, 16]. Also, refer to Appendix A for the identification of symbols.

$$EI_S \frac{\partial^4 \bar{X}(y,t)}{\partial y^4} + \rho S \frac{\partial^2 \bar{X}(y,t)}{\partial t^2} - \left[\rho I_S + EI_S \frac{\rho}{\kappa G}\right] \frac{\partial^4 \bar{X}(y,t)}{\partial t^2 \partial y^2} + \rho I_S \frac{\rho}{\kappa G} \frac{\partial^4 \bar{X}(y,t)}{\partial t^4} = 0. \quad (1)$$

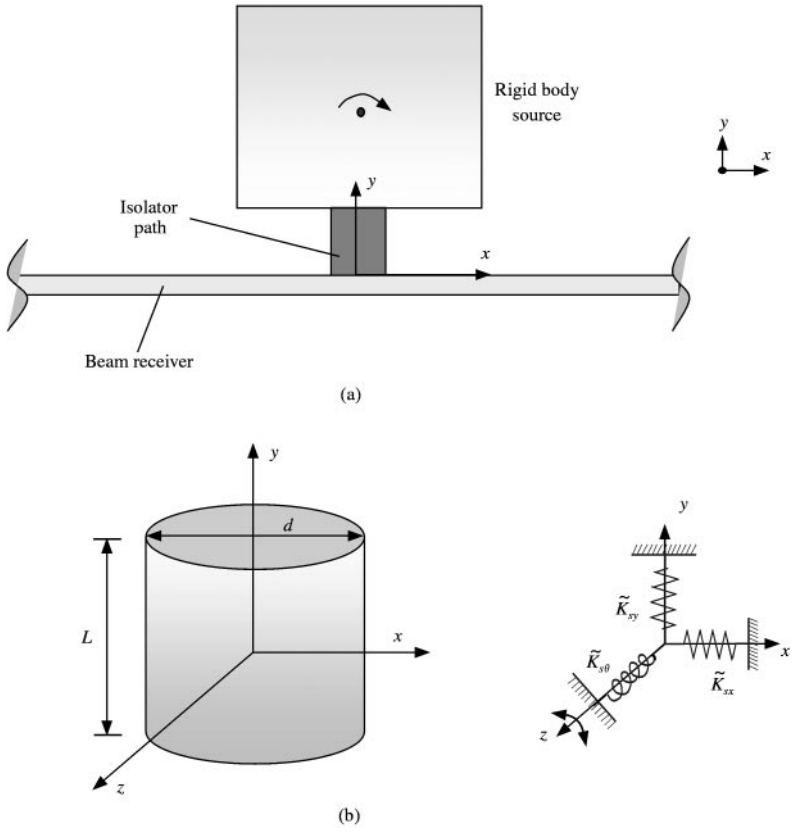

Figure 1. Vibration transmission via multi-dimensional motions of an isolator. (a) System configuration with a beam receiver; (b) a cylindrical isolator with static stiffness components used for parametric studies. Here, K_{Sy} is the axial (longitudinal or compressional) stiffness, K_{Sx} is the lateral (shear) stiffness and $K_{S\theta}$ is the rotational stiffness.

Assuming $\bar{X}(y, t) = X(y)e^{j\omega t}$, the equation for $X(y)$ is

$$\frac{d^4X(y)}{dy^4} + k^4r_g^2\left[\frac{1}{\kappa}\frac{E}{G} + 1\right]\frac{d^2X(y)}{dy^2} + k^4\left[k^4r_g^4\frac{1}{\kappa}\frac{E}{G} - 1\right]X(y) = 0. \tag{2}$$

Here, k is the flexural wave number given by $k^4 = \omega^2\rho S/(EI_S)$ and $r_g = (I_S/S)^{1/2}$ is the radius of gyration. The above equation is rewritten by introducing non-dimensional parameters $\xi = y/L$, $\upsilon_1 = (r_g^2E)/(\kappa L^2G)$, and $\upsilon_2 = r_g^2/L^2$:

$$\frac{d^4X(\xi)}{d\xi^4} + [kL]^4[\upsilon_1 + \upsilon_2]\frac{d^2X(\xi)}{d\xi^2} + [kL]^4[[kL]^4\upsilon_1\upsilon_2 - 1]\,X(\xi) = 0. \tag{3}$$

Equation (3) is a linear ordinary differential equation of the fourth order, and has four roots (λ) given by $X(\xi) = Ae^{(\lambda L)\xi}$, where A is an arbitrary constant. Substitution of the assumed exponential solution into equation (3) leads to the following characteristic equation and two

categories of roots [16]:

$$(\lambda L)^4 + [kL]^4[\upsilon_1 + \upsilon_2](\lambda L)^2 + [kL]^4[[kL]^4\upsilon_1\upsilon_2 - 1] = 0, \tag{4a}$$

$$(\lambda_1 L)^2 = \frac{-(kL)^4(\upsilon_1 + \upsilon_2) - \sqrt{(kL)^8(\upsilon_1 - \upsilon_2)^2 + 4(kL)^4}}{2}, \tag{4b}$$

$$(\lambda_2 L)^2 = \frac{-(kL)^4(\upsilon_1 + \upsilon_2) + \sqrt{(kL)^8(\upsilon_1 - \upsilon_2)^2 + 4(kL)^4}}{2}, \tag{4c}$$

$$(\lambda_1 L)^2 + (\lambda_2 L)^2 = (kL)^4(\upsilon_1 + \upsilon_2), \qquad (\lambda_1 L)^2(\lambda_2 L)^2 = (kL)^4[(kL)^4\upsilon_1\upsilon_2 - 1]. \tag{4d, e}$$

The $(\lambda_1 L)^2$ root is always negative but the $(\lambda_2 L)^2$ solution is positive only when $R < 1$, where $R = (\rho I_S \omega^2)/(\kappa SG)$. However, $(\lambda_2 L)^2$ will be negative when $R > 1$ according to the following relationship:

$$[[kL]^4\upsilon_1\upsilon_2 - 1] = \frac{\rho I_S \omega^2}{\kappa SG} - 1 = R - 1. \tag{5}$$

Therefore, when $R > 1$, solutions are expressed only in the trigonometric form. Otherwise, for $R < 1$, solutions must be expressed using both trigonometric and hyperbolic forms. It is believed that the $R > 1$ case is related to an extremely high-frequency phenomenon, and thus previously not considered to be of any practical interest in structural dynamics [4]. However, our study for a rubber-like material shows that the transition for this occurs at moderately high frequencies. The solution changes at the transition frequency ω_T, that is

$$\omega_T = \sqrt{\kappa SG/(\rho I_S)}. \tag{6}$$

The steady state response in flexural motion for the case when $R < 1$ is

$$X(\xi) = A_1 e^{-j[(\tau L)\xi]} + B_1 e^{j[(\tau L)\xi]} + C_1 e^{-[(\varepsilon_1 L)\xi]} + D_1 e^{[(\varepsilon_1 L)\xi]}, \text{ or} \tag{7a}$$

$$X(\xi) = A_1 \sin[(\tau L)\xi] + B_1 \cos[(\tau L)\xi] + C_1 \sinh[(\varepsilon_1 L)\xi] + D_1 \cosh[(\varepsilon_1 L)\xi]. \tag{7b}$$

In the above expressions, the following parameters are introduced:

$$(\tau L)^2 = -(\lambda_1 L)^2, \qquad (\varepsilon_1 L)^2 = (\lambda_2 L)^2. \tag{8a, b}$$

Next, for the case when $R > 1$, the steady state response in flexural motion is

$$X(\xi) = A_2 e^{-j[(\tau L)\xi]} + B_2 e^{j[(\tau L)\xi]} + C_2 e^{-j[(\varepsilon_2 L)\xi]} + D_2 e^{j[(\varepsilon_2 L)\xi]}, \text{ or} \tag{9a}$$

$$X(\xi) = A_2 \sin[(\tau L)\xi] + B_2 \cos[(\tau L)\xi] + C_2 \sin[(\varepsilon_2 L)\xi] + D_2 \cos[(\varepsilon_2 L)\xi]. \tag{9b}$$

The following parameter is used in equations (9a, b) along with equation (8a):

$$(\varepsilon_2 L)^2 = -(\lambda_2 L)^2. \tag{10}$$

Note that the $(\tau L)^2$, $(\varepsilon_1 L)^2$ and $(\varepsilon_2 L)^2$ are positive for an undamped structure. Hence, the arguments of trigonometric and hyperbolic terms in equations (7b) and (9b) remain real valued. Therefore, the decaying nearfield components do not appear in the solution for the $R > 1$ case. Conversely, the solution for the $R < 1$ case consists of both propagating and nearfield wave components. For a damped structure, it is more convenient to employ the

following general expression along with equations (4b, c) without separating the two cases since the expansion of exponential terms with a complex argument becomes tedious:

$$X(\xi) = A\mathrm{e}^{[(\lambda_1 L)\xi]} + B\mathrm{e}^{-[(\lambda_1 L)\xi]} + C\mathrm{e}^{[(\lambda_2 L)\xi]} + D\mathrm{e}^{-[(\lambda_2 L)\xi]}. \tag{11}$$

The harmonic responses are obtained by applying the following boundary conditions: a harmonic force $f_0\mathrm{e}^{\mathrm{j}\omega t}$ is applied at $y = 0$ and the other end ($y = L$) is free.

$$\frac{\kappa SG\upsilon_1}{[1-(kL)^4\upsilon_1\upsilon_2]L}\left[\frac{\mathrm{d}^3X(0)}{\mathrm{d}\xi^3} + (kL)^4(\upsilon_1+\upsilon_2)\frac{\mathrm{d}X(0)}{\mathrm{d}\xi}\right] = f_0, \tag{12a}$$

$$-\frac{EI_S}{L^2}\left[\frac{\mathrm{d}^2X(0)}{\mathrm{d}\xi^2} + \upsilon_1(kL)^4X(0)\right] = 0, \tag{12b}$$

$$-\frac{\kappa SG\upsilon_1}{[1-(kL)^4\upsilon_1\upsilon_2]L}\left[\frac{\mathrm{d}^3X(1)}{\mathrm{d}\xi^3} + (kL)^4(\upsilon_1+\upsilon_2)\frac{\mathrm{d}X(1)}{\mathrm{d}\xi}\right] = 0, \tag{12c}$$

$$-\frac{EI_S}{L^2}\left[\frac{\mathrm{d}^2X(1)}{\mathrm{d}\xi^2} + \upsilon_1(kL)^4X(1)\right] = 0. \tag{12d}$$

Further, we simplify the above equations (12a–d) as

$$\frac{EI_S(kL)^4}{L^3(\lambda_1 L)(\lambda_2 L)}[(\lambda_2 L)A - (\lambda_2 L)B + (\lambda_1 L)C - (\lambda_1 L)D] = f_0, \tag{13a}$$

$$-\frac{EI_S}{L^2}[\mu A + \mu B + \chi C + \chi D] = 0, \tag{13b}$$

$$-\frac{EI_S(kL)^4}{L^3(\lambda_1 L)(\lambda_2 L)}[(\lambda_2 L)\mathrm{e}^{(\lambda_1 L)}A - (\lambda_2 L)\mathrm{e}^{-(\lambda_1 L)}B + (\lambda_1 L)\mathrm{e}^{(\lambda_2 L)}C - (\lambda_1 L)\mathrm{e}^{-(\lambda_2 L)}D] = 0, \tag{13c}$$

$$-\frac{EI_S}{L^2}[\mu\mathrm{e}^{(\lambda_1 L)}A + \mu\mathrm{e}^{-(\lambda_1 L)}B + \chi\mathrm{e}^{(\lambda_2 L)}C + \chi\mathrm{e}^{-(\lambda_2 L)}D] = 0, \tag{13d}$$

where

$$\mu = [(kL)^4\upsilon_1 + (\lambda_1 L)^2], \qquad \chi = [(kL)^4\upsilon_1 + (\lambda_2 L)^2]. \tag{14a, b}$$

Only the slope θ_B due to bending is considered since the shear deformation does not produce any rotation:

$$\theta_B(\xi) = \frac{\mu}{L(\lambda_1 L)}A\mathrm{e}^{(\lambda_1 L)\xi} - \frac{\mu}{L(\lambda_1 L)}B\mathrm{e}^{-(\lambda_1 L)\xi} + \frac{\chi}{L(\lambda_2 L)}C\mathrm{e}^{(\lambda_2 L)\xi} - \frac{\chi}{L(\lambda_2 L)}D\mathrm{e}^{-(\lambda_2 L)\xi}. \tag{15}$$

Like the harmonic force excitation case, replacing the right-hand sides of equations (13a) and (13b) by 0 and q_0, respectively, yields steady state responses when a harmonic moment

$q_0 e^{j\omega t}$ is applied at $y = 0$. In a similar manner, the driving point and transfer mobility components for the case of force and moment excitations at $y = L$ can be obtained by using the following reciprocity and physical symmetry conditions:

$$\frac{v_L}{f_L} = \frac{v_0}{f_0}, \quad \frac{w_L}{f_L} = -\frac{w_0}{f_0}, \quad \frac{v_L}{q_L} = -\frac{v_0}{q_0}, \quad \frac{w_L}{q_L} = \frac{w_0}{q_0}, \tag{16a–d}$$

$$\frac{v_0}{f_L} = \frac{v_L}{f_0}, \quad \frac{w_0}{f_L} = \frac{v_L}{q_0}, \quad \frac{v_0}{q_L} = \frac{w_L}{f_0}, \quad \frac{w_0}{q_L} = \frac{w_L}{q_0}. \tag{16e–h}$$

Here, the subscripts 0 and L imply response or excitation at $y = 0$ and L respectively. Further, v and w are the translational and rotational velocity amplitudes respectively. The resulting mobility matrix that incorporates the finite Timoshenko beam can be directly used to determine the harmonic response of any combined system by using the mobility synthesis formulation. Note that the mobility synthesis method uses free boundary conditions for sub-systems [19].

3.2. CHARACTERISTIC MOBILITIES OF A SEMI-INFINITE TIMOSHENKO BEAM

It is of interest to observe the behavior of a semi-infinite Timoshenko beam since the mobility of a finite Timoshenko beam shows a completely different tendency for the second type of solution at higher frequencies when compared with lower frequencies. Rewrite equation (3) using the parameters $\upsilon_{1-} = (r_g^2 E)/(\kappa G)$ and $\upsilon_{2-} = r_g^2$ as

$$\frac{d^4 X(y)}{dy^4} + k^4 [\upsilon_{1-} + \upsilon_{2-}] \frac{d^2 X(y)}{dy^2} + k^4 [k^4 \upsilon_{1-} \upsilon_{2-} - 1] X(y) = 0. \tag{17}$$

Similar to the finite beam case, it is more convenient to adopt the following solution for a damped semi-infinite structure:

$$X(y) = A e^{-[\lambda_{1-} y]} + C e^{-[\lambda_{2-} y]}, \tag{18a}$$

$$\lambda_{1-}^2 = \frac{-k^4(\upsilon_{1-} + \upsilon_{2-}) - \sqrt{k^8(\upsilon_{1-} - \upsilon_{2-})^2 + 4k^4}}{2}, \tag{18b}$$

$$\lambda_{2-}^2 = \frac{-k^4(\upsilon_{1-} + \upsilon_{2-}) + \sqrt{k^8(\upsilon_{1-} - \upsilon_{2-})^2 + 4k^4}}{2}. \tag{18c}$$

For the case when $R < 1$, the harmonic response for a semi-infinite beam is

$$X(y) = A_1 e^{-j[\tau_{1-} y]} + C_1 e^{-[\varepsilon_{1-} y]}, \qquad \tau_{1-}^2 = -\lambda_{1-}^2, \qquad \varepsilon_{1-}^2 = \lambda_{2-}^2. \tag{19a–c}$$

Next, when $R > 1$, the harmonic response is

$$X(y) = A_2 e^{-j[\tau_{1-} y]} + C_2 e^{-j[\varepsilon_{2-} y]}, \qquad \varepsilon_{2-}^2 = -\lambda_{2-}^2. \tag{20a, b}$$

The characteristic mobilities of a semi-infinite Timoshenko beam are obtained by applying the force and moment excitations to equation (18a) at $y = 0$:

$$\frac{v_0}{f_0} = \frac{\lambda_{1-}\lambda_{2-}[\upsilon_{1-} - \upsilon_{2-}]\mathrm{j}\omega}{EI[\lambda_{2-}\chi_- - \mu_-\lambda_{1-}]}, \qquad \frac{w_0}{q_0} = \frac{[\chi_- - \mu_-]\mathrm{j}\omega}{EI[\lambda_{2-}\chi_- - \mu_-\lambda_{1-}]}, \tag{21a, b}$$

$$\frac{w_0}{f_0} = \frac{v_0}{q_0} = \frac{[\lambda_{1-} - \lambda_{2-}]\mathrm{j}\omega}{EI[\lambda_{2-}\chi_- - \mu_-\lambda_{1-}]}. \tag{21c}$$

$$\mu_- = [k^4\upsilon_{1-} + \lambda_{1-}^2], \qquad \chi_{1-} = [k^4\upsilon_{1-} + \lambda_{2-}^2]. \tag{21d, e}$$

3.3. TYPICAL MOBILITY SPECTRUM

The effects of shear deformation and rotary inertia on the characteristic mobilities for a semi-infinite rubber beam are examined and shown in Figure 2. Calculations are also conducted by letting $\upsilon_{2-} = 0$ in equations (21a–c) for a Euler beam with shear deformation only and by letting $\upsilon_{1-} = 0$ for a Euler beam with rotary inertia only. The example case considers a rubber beam with circular shape. The spectrally invariant material properties and dimensions of the beam that is considered as an isolator are shown in Table 1. It is observed from Figure 2 that the inclusion of shear deformation increases the magnitudes of force and moment mobilities. Conversely, the rotary inertia decreases the magnitudes of force and moment mobilities. Further, the shear deformation does not affect the coupling mobility of Figure 2(b) that is frequency-invariant for the Euler beam model and the one with shear deformation only. For this circular rubber beam, ω_T is approximately 1·7 kHz and the nature of the solution changes beyond this transition. Beyond ω_T, the characteristic force and moment mobilities of the Timoshenko beam model remain frequency-invariant as the frequency increases, unlike the Euler beam model. Further, the coupling mobility decreases by the rotary inertia effect and one of the Timoshenko beam solution decreases more rapidly beyond ω_T. Also, the coupling mobilities of the Euler beam with or without shear deformation are the same as shown in Figure 2(b). The transfer mobilities of a finite circular rubber beam are also computed using the material properties and dimensions of the isolator in Table 1, as shown in Figure 3 for loss factors (η) 0·001 and 0·3. Unlike the transfer mobilities of the Euler beam, anti-resonances appear in the Timoshenko beam case as shown in Figure 3. Similar to the characteristic mobilities of a semi-infinite Timoshenko beam, the characteristics of force and moment mobilities for a finite beam remain frequency-invariant. The coupling mobility of a finite beam, however, decreases in an asymptotic manner as the frequency increases beyond ω_T, as shown in Figure 3.

4. VIBRATION POWER TRANSMITTED TO AN INFINITE BEAM RECEIVER

4.1. SYSTEM CONFIGURATION

The vibrational behavior is examined for an isolation system (Figure 1(a)) with an infinite beam receiver. Harmonic excitation is applied at the mass center of a cubic rigid body. A circular isolator is shown in Figure 1(b) along with vibration components transmitted through the path. The isolator is modelled using the Timoshenko beam theory (flexural motion) and the wave equation (longitudinal motion). Note that the coupling mobility does not exist for an infinite beam receiver. However, a coupling arises because the motion (or force) in shear direction of an isolator is coupled with the longitudinal direction of a receiver

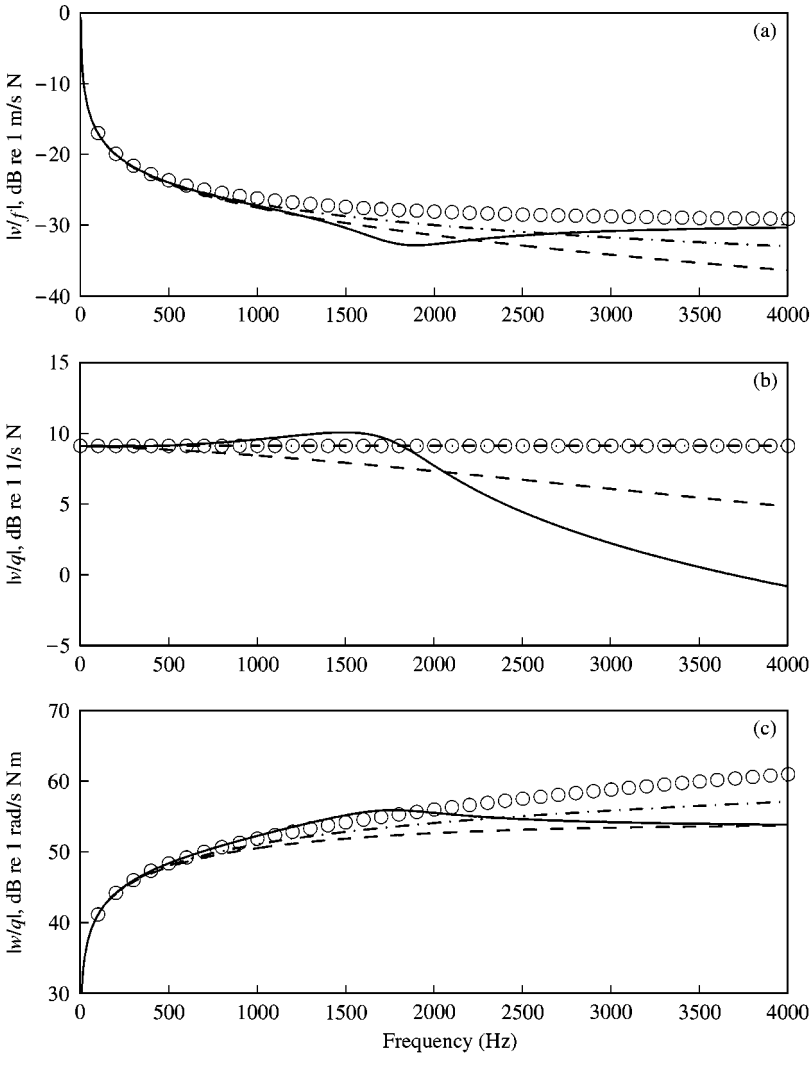

Figure 2. Characteristic mobilities of a semi-infinite beam. (a) Force mobility $|v/f|$; (b) coupling mobility $|v/q|$; (c) moment mobility $|w/q|$: ——, Timoshenko beam; ○, Euler beam with shear deformation; - - - - -, Euler beam with rotary inertia; – – – – –, classical Euler beam. Here, ω_T is 1700 Hz.

beam. The following measures of vibration isolation performance are examined: (1) total vibration power (Π) transmitted to receiver; (2) transmission efficiency (Γ = ratio of transmitted power to input power); and (3) effectiveness of vibration power (Ξ = ratio of the net transmitted power with mount to the net transmitted power without mount). Steady state responses of an isolator path for axial (y) and flexural (x and θ) motions are, respectively, as follows where the subscript P implies the isolator path. The second subscript gives the direction x or y. Further, A, B, C and D are arbitrary constants and k_{PL} is the longitudinal wave number of the isolator path.

$$\bar{Y}_P(y, t) = Y_P(y)\,e^{j\omega t} = \{A_{Py}e^{-jk_{PL}y} + B_{Py}e^{jk_{PL}y}\}\,e^{j\omega t}, \tag{22a}$$

$$\bar{X}_P(y, t) = X_P(y)\,e^{j\omega t} = \{A_{Px}e^{[\tau y]} + B_{Px}e^{-[\tau y]} + C_{Px}e^{[\varepsilon y]} + D_{Px}e^{-[\varepsilon y]}\}\,e^{j\omega t}. \tag{22b}$$

TABLE 1

Material properties and dimensions of source, isolator and receiver system

Property or dimension	Source (cubic rigid body)	Isolator: baseline (circular beam)	Receiver (rectangular beam)
m (kg)	1	—	—
E (MPa)	—	16·2	$6{\cdot}688 \times 10^4$
G (MPa)	—	5	—
η	—	0·3	0·001
ρ (kg/m^3)	—	1000	2723
Dimensions in mm	$L = 50$	$L = 30$ $r = 12$	$L = 670$ (finite beam) $b = 100$ and $t = 10$ (finite or infinite beam)

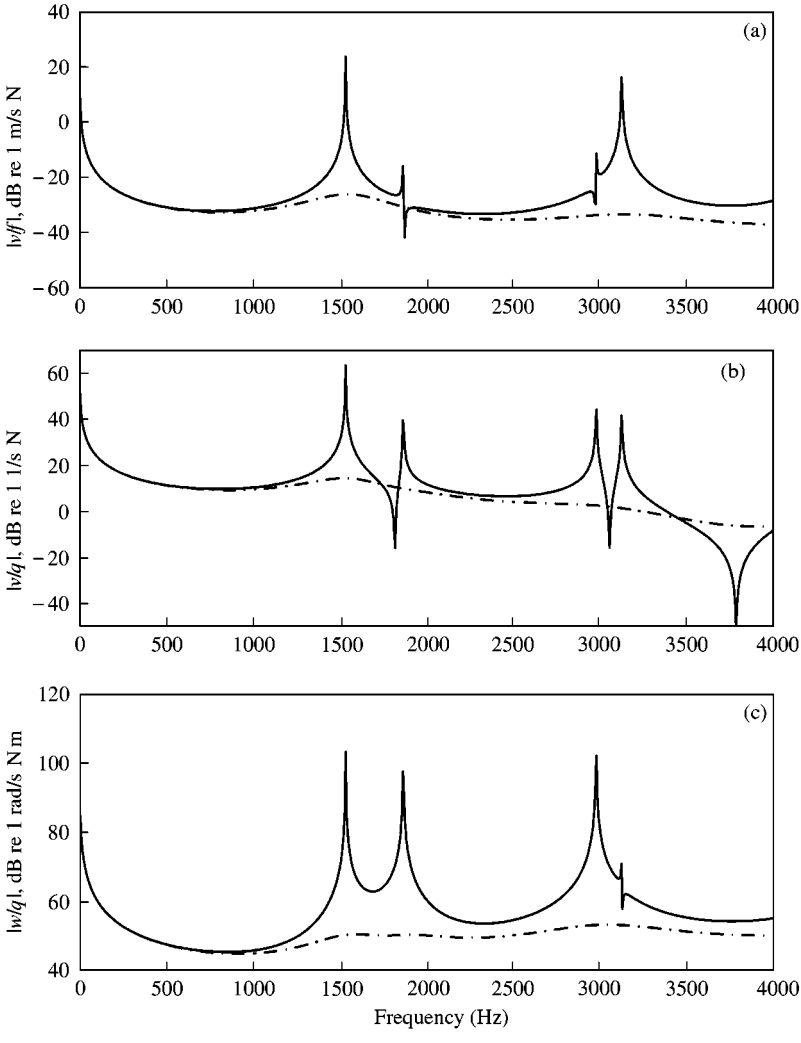

Figure 3. Transfer mobilities of a finite Timoshenko beam with free boundaries. (a) Force mobility $|v/f|$; (b) coupling mobility $|v/q|$; (c) moment mobility $|w/q|$: ——, $\eta = 0{\cdot}001$; – – – – –, $\eta = 0{\cdot}3$. Here, ω_T is 1700 Hz.

Also, harmonic responses of an infinite beam for axial (x) and flexural (y) motions are, respectively, as follows where the subscript R denotes the receiver beam. The second subscripts R and L in equation (23) are used for the right-travelling and the left-travelling waves, respectively, and the third subscript implies the direction x or y. Further, k_{RL} and k_{RB} are the longitudinal and bending wave numbers of the receiver beam respectively.

$$\bar{X}_{RL}(x,t) = X_{RL}(x)\,\mathrm{e}^{\mathrm{j}\omega t} = A_{RLx}\mathrm{e}^{\mathrm{j}k_{RL}x}\mathrm{e}^{\mathrm{j}\omega t}, \tag{23a}$$

$$\bar{X}_{RR}(x,t) = X_{RR}(x)\,\mathrm{e}^{\mathrm{j}\omega t} = A_{RRx}\mathrm{e}^{-\mathrm{j}k_{RL}x}\mathrm{e}^{\mathrm{j}\omega t}, \tag{23b}$$

$$\bar{Y}_{RL}(x,t) = Y_{RL}(x)\,\mathrm{e}^{\mathrm{j}\omega t} = \{A_{RLy}\mathrm{e}^{\mathrm{j}[k_{RB}x]} + B_{RLy}\mathrm{e}^{[k_{RB}x]}\}\mathrm{e}^{\mathrm{j}\omega t}, \tag{23c}$$

$$\bar{Y}_{RR}(x,t) = Y_{RR}(x)\,\mathrm{e}^{\mathrm{j}\omega t} = \{A_{RRy}\mathrm{e}^{-\mathrm{j}[k_{RB}x]} + B_{RRy}\mathrm{e}^{-[k_{RB}x]}\}\mathrm{e}^{\mathrm{j}\omega t}. \tag{23d}$$

The governing equations in frequency domain are described as follows where the ubiquitous term $e^{\mathrm{j}\omega t}$ is dropped. Here, I_m is the moment of inertia corresponding to a rigid body source and h is the rigid body location where the isolator is attached. Also, f_y and q are harmonic force and moment excitation amplitudes, respectively, at frequency ω.

$$X_{RL}(0) = X_{RR}(0), \qquad Y_{RL}(0) = Y_{RR}(0), \tag{24a, b}$$

$$X_{RL}(0) = X_P(0), \qquad Y_{RL}(0) = Y_P(0), \tag{24c, d}$$

$$\frac{\mathrm{d}Y_{RL}(0)}{\mathrm{d}x} = \frac{\mathrm{d}Y_{RR}(0)}{\mathrm{d}x}, \qquad \frac{\mathrm{d}Y_{RL}(0)}{\mathrm{d}x} = -\frac{\mathrm{d}X_P(0)}{\mathrm{d}y}, \tag{24e, f}$$

$$E_R I_{RS}\left[\frac{\mathrm{d}^3 Y_{RR}(0)}{\mathrm{d}x^3} - \frac{\mathrm{d}^3 Y_{RL}(0)}{\mathrm{d}x^3}\right] = S_P E_P \frac{\mathrm{d}Y_P(0)}{\mathrm{d}y}, \tag{24g}$$

$$\frac{\kappa_P S_P G_P \upsilon_1}{1-(k_P L_P)^4 \upsilon_1 \upsilon_2}\left[L_P^2 \frac{\mathrm{d}^3 X_P(0)}{\mathrm{d}y^3} + (k_P L_P)^4(\upsilon_1+\upsilon_2)\frac{\mathrm{d}X_P(0)}{\mathrm{d}y}\right] = S_R E_R\left[\frac{\mathrm{d}X_{RR}(0)}{\mathrm{d}x} - \frac{\mathrm{d}X_{RL}(0)}{\mathrm{d}x}\right], \tag{24h}$$

$$E_R I_{RS}\left[\frac{\mathrm{d}^2 Y_{RL}(0)}{\mathrm{d}x^2} - \frac{\mathrm{d}^2 Y_{RR}(0)}{\mathrm{d}x^2}\right] = E_P I_{PS}\left[\frac{\mathrm{d}^2 X_P(0)}{\mathrm{d}y^2} + \frac{\upsilon_1}{L^2}(k_P L)^4 X_P(0)\right], \tag{24i}$$

$$-\frac{\kappa_P S_P G_P \upsilon_1}{1-(k_P L_P)^4 \upsilon_1 \upsilon_2}\left[L_P^2 \frac{\mathrm{d}^3 X_P(L_P)}{\mathrm{d}y^3} + (k_P L_P)^4(\upsilon_1+\upsilon_2)\frac{\mathrm{d}X_P(L_P)}{\mathrm{d}y}\right] - m\omega^2 X_P(L_P) - mh\omega^2 \frac{\mathrm{d}X_P(L_P)}{\mathrm{d}y} = 0, \tag{24j}$$

$$-m\omega^2 Y_P(L_P) + S_P E_P \frac{\mathrm{d}Y_P(L_P)}{\mathrm{d}y} = f_y, \tag{24k}$$

$$-(I_{mG}+mh^2)\,\omega^2 \frac{\mathrm{d}X_P(L_P)}{\mathrm{d}y} - mh\omega^2 X_P(L_P) + E_P I_{PS}\left[\frac{\mathrm{d}^2 X_P(L_P)}{\mathrm{d}y^2} + \frac{\upsilon_1}{L^2}(k_P L)^4 X_P(L_P)\right] = q. \tag{24l}$$

Harmonic responses for each excitation are separately obtained by solving the boundary conditions (24a–l) in terms of the arbitrary constants A, B, C and D. When the harmonic force f_y is applied at the mass center of the rigid body, the steady state responses are obtained by letting $q = 0$ in equation (24l). Similarly, the right-hand side of (24k) is set to 0 when q is applied at the mass center of rigid body. Internal axial (F), shear (V) forces and moment (M) at interfacial location between an isolator and an infinite beam receiver are calculated as follows using the resulting arbitrary constants:

$$F_R = S_R E_R \left[\frac{\mathrm{d}X_{RL}(0)}{\mathrm{d}x} - \frac{\mathrm{d}X_{RR}(0)}{\mathrm{d}x} \right], \qquad M_R = E_R I_{RS} \left[\frac{\mathrm{d}^2 Y_{RL}(0)}{\mathrm{d}x^2} - \frac{\mathrm{d}^2 Y_{RR}(0)}{\mathrm{d}x^2} \right], \quad (25a, b)$$

$$V_R = - E_R I_{RS} \left[\frac{\mathrm{d}^3 Y_{RL}(0)}{\mathrm{d}x^3} - \frac{\mathrm{d}^3 Y_{RR}(0)}{\mathrm{d}x^3} \right]. \quad (25c)$$

The time-averaged vibrational power (Π) components transmitted to an infinite beam receiver are obtained by using the resulting harmonic responses and interfacial forces (F and V) and moment (M). Define Π_x, Π_y and Π_θ as the lateral (x), axial (y) and rotational (θ) power components, respectively:

$$\Pi_x(\omega) = \frac{1}{2} \mathrm{Re}[\tilde{F}(\omega)\, \tilde{v}_x^*(\omega)] = \frac{1}{2} \mathrm{Re}[\tilde{v}_x(\omega)\, \tilde{F}^*(\omega)], \quad (26a)$$

$$\Pi_y(\omega) = \frac{1}{2} \mathrm{Re}[\tilde{V}(\omega)\, \tilde{v}_y^*(\omega)] = \frac{1}{2} \mathrm{Re}[\tilde{v}_y(\omega)\, \tilde{V}^*(\omega)], \quad (26b)$$

$$\Pi_\theta(\omega) = \frac{1}{2} \mathrm{Re}[\tilde{M}(\omega)\, \tilde{w}^*(\omega)] = \frac{1}{2} \mathrm{Re}[\tilde{w}(\omega)\, \tilde{M}^*(\omega)]. \quad (26c)$$

Here, v_x, v_y and w are the axial (shear direction x for isolator), vertical (axial direction y for isolator) and rotational (θ) velocity amplitudes of the receiver beam respectively. Finally, the total vibration power transmitted to a receiver beam is

$$\Pi_{Total}(\omega) = \Pi_x(\omega) + \Pi_y(\omega) + \Pi_\theta(\omega). \quad (27)$$

Additionally, define the following measures of vibration isolation performance:

$$\Gamma(\omega) = \frac{\Pi_{Total}(\omega)}{\Pi_{IN}(\omega)}, \qquad \Xi(\omega) = \frac{\Pi_{Total,\,With}(\omega)}{\Pi_{Total,\,Without}(\omega)}, \quad (28a, b)$$

where Π_{IN} is the harmonic power supplied to a rigid body source. For force (f_y) and moment (q) excitation cases, we find

$$\Pi_{IN}(\omega) = f_y\, \mathrm{j}\omega Y_P(L_P), \qquad \Pi_{IN}(\omega) = q\, \mathrm{j}\omega \frac{\mathrm{d}X_P(L_P)}{\mathrm{d}y}. \quad (29a, b)$$

The governing equations of the system without an isolator are

$$X_{RL}(0) = X_{RR}(0), \qquad Y_{RL}(0) = Y_{RR}(0), \qquad \frac{\mathrm{d}Y_{RL}(0)}{\mathrm{d}x} = \frac{\mathrm{d}Y_{RR}(0)}{\mathrm{d}x}, \quad (30a–c)$$

$$- m\omega^2 X_R(0) + mh\omega^2 \frac{\mathrm{d}Y_R(0)}{\mathrm{d}x} + S_R E_R \left[\frac{\mathrm{d}X_{RL}(0)}{\mathrm{d}x} - \frac{\mathrm{d}X_{RR}(0)}{\mathrm{d}x} \right] = 0, \quad (30d)$$

$$-m\omega^2 Y_R(0) + E_R I_{RS}\left[\frac{\mathrm{d}^3 Y_{RR}(0)}{\mathrm{d}x^3} - \frac{\mathrm{d}^3 Y_{RL}(0)}{\mathrm{d}x^3}\right] = f_y, \tag{30e}$$

$$-(I_{mG} + mh^2)\,\omega^2 \frac{\mathrm{d}Y_{RL}(0)}{\mathrm{d}x} - mh\omega^2 X_R(0) + E_R I_{RS}\left[\frac{\mathrm{d}^2 Y_{RL}(0)}{\mathrm{d}x^2} - \frac{\mathrm{d}^2 Y_{RR}(0)}{\mathrm{d}x^2}\right] = q. \tag{30f}$$

Similar to the system with an isolator, harmonic responses of a receiver beam are obtained using equations (23a–d). Further, moment, shear force of an infinite beam and transmitted power are obtained using equations (25a–c) and (26, 27).

Material properties of the isolator are listed in Table 1. Young's modulus E_P for a rubber material is found from the relation $E_P = 3G_P(1 + QT^2)$, where Q is an empirical constant and T is the shape factor. For a circular rubber cylinder, Q is 2 and T is equal to $2r/(4L_P)$, where r and L_P are the radius and length of the isolator beam respectively [4]. Also, a frequency-invariant loss factor η_P is included in the calculation with the complex-valued Young·s modulus as $\tilde{E}_P = E_P(1 + \mathrm{j}\eta_P)$ to incorporate hysteretic damping within the isolator. Material properties of the receiver beam are, as well as the dimensions of source, also shown in Table 1. A loss factor η_R of 0·001 is used to represent a lightly damped structure and is included in the complex-valued $\tilde{E}_R$. Given the system properties, the effects of shear deformation and rotary inertia of an isolator on the vibration power transmitted to receiver are examined. Further, the effects of isolator material and geometric properties are investigated.

4.2. EXAMINATION OF ALTERNATE ISOLATOR MODELS

Vibration power transmission to receiver is analyzed up to 4 kHz when a harmonic moment is applied at the source. The following four alternate isolator models are employed to describe the flexural vibration power transmitted to an infinite beam receiver: Timoshenko beam, Euler beam with shear deformation, Euler beam with rotary inertia and Euler beam models. Total vibration power (Π) transmitted to a receiver beam is shown in Figure 4 along with the transmission power efficiency (Γ) and the effectiveness (Ξ) of vibration power. First, it is observed that rotary inertia does not significantly affect the vibration power transmission below ω_T, that is, around 1·7 kHz. Note that the measures of Figure 4 based on the Euler beam isolator with rotary inertia are similar to those using the Euler beam below ω_T. Beyond ω_T, the discrepancies between measures based on those alternate models are pronounced as frequency increases. Further, it is seen that the Euler beam model with shear deformation provides a closer representation of the Timoshenko beam isolator even beyond ω_T even though there exist small disagreements between them. However, large discrepancies between the Timoshenko beam and Euler beam formulations without shear deformation are found. Normalized power components with respect to the total actual power transmitted to the receiver beam are shown in Figure 5. As mentioned earlier, since each vibration power component is decoupled from the others in total power, each power component is always positive in this case. Only flexural motions are transmitted through the mount in this particular example case and therefore only the lateral (shear direction of the mount) and rotational power components control the total vibration power transmission. It is observed in Figure 5 that the lateral power component is larger than the rotational component when the isolator is modelled using the Timoshenko beam or Euler beam with shear deformation. Also, the total vibration power with the Euler beam isolator models with and without rotary inertia is almost equally divided into lateral and rotational components.

4.3. EFFECT OF ISOLATOR PROPERTIES ON VIBRATION POWER TRANSMISSION

In order to understand the effect of isolator properties, it is useful to examine the static stiffnesses (K_S) of an isolator. It should be noted that flexural stiffnesses have to be dealt with in a matrix form since there exist coupling terms between lateral (shear x) and rotational (θ) stiffnesses. The static stiffnesses of a Euler beam are well known and written here as follows, where the subscript E represents the Euler beam:

$$\begin{bmatrix} f \\ q \end{bmatrix} = \mathbf{K}_{SE} \begin{bmatrix} X \\ \theta \end{bmatrix} = \begin{bmatrix} -12EI/L^3 & -6EI/L^2 \\ 6EI/L^2 & 2EI/L \end{bmatrix} \begin{bmatrix} X \\ \theta \end{bmatrix}. \tag{31}$$

For the static stiffnesses of a Timoshenko beam, the following governing equations are used for the sake of convenience:

$$-GS\kappa \left[\frac{\partial X^2(y)}{\partial y^2} - \frac{\partial \theta_B(y)}{\partial y} \right] = \mathrm{w}(x), \tag{32a}$$

$$GS\kappa \left[\frac{\partial X(y)}{\partial y} - \theta_B(y) \right] + EI_S \frac{\partial^2 \theta_B(y)}{\partial y^2} = 0. \tag{32b}$$

Here, $\mathrm{w}(x)$ is the load intensity function and θ_B is the slope due only to bending of the beam. Combining the above equations and including the inertia terms yield equation (1) that has been previously used for the harmonic response. The static stiffnesses of the Timoshenko beam are obtained by using the singularity function for load intensity and displacement functions and applying the blocked end boundary condition at one end. The resulting static stiffness matrix is as follows, where the subscript T stands for the Timoshenko beam:

$$\begin{bmatrix} f \\ q \end{bmatrix} = \mathbf{K}_{ST} \begin{bmatrix} X \\ \theta_B \end{bmatrix} = \begin{bmatrix} -\dfrac{1}{L^3/12EI_S + L/GS\kappa} & -\dfrac{1}{L^2/6EI_S + 2/GS\kappa} \\ \dfrac{1}{L^2/6EI_S + 2/GS\kappa} & \dfrac{1}{L/3EI_S + 4/GS\kappa L} - \dfrac{EI_S}{L} \end{bmatrix} \begin{bmatrix} X \\ \theta_B \end{bmatrix}. \tag{33}$$

From the above equation, the flexural stiffness terms can be interpreted in terms of a lumped system that combines the elastic elements due to bending and shear in series. Further, it is seen that $\mathbf{K}_{ST} \to \mathbf{K}_{SE}$ when $GS\kappa \to \infty$ in equation (33). Equation (33) is expanded by using the relationships $I_S = Sr_g^2$ and $G = E/2(1+\nu)$, and the $\mathbf{K}_{ST}$ is rewritten as follows where K_{Sx}, K_{Sc} and $K_{S\theta}$ represent the static shear, coupling and rotational stiffnesses, respectively:

$$\mathbf{K}_{ST} = \begin{bmatrix} K_{Sx} & K_{Sc} \\ K_{Sc} & K_{S\theta} \end{bmatrix} = \frac{GS}{L} \frac{4r_g^2\kappa(1+\nu)}{[\kappa L^2 + 24(1+\nu)r_g^2]} \begin{bmatrix} -6 & -3L \\ 3L & L^2[1 - 12(1+\nu)r_g^2/\kappa L^2] \end{bmatrix}. \tag{34}$$

On the other hand, the static axial (y) stiffness is

$$K_{Sy} = \frac{ES}{L} = \frac{2GS(1+\nu)}{L}. \tag{35}$$

Note that G (or E) is common to all stiffness terms. The system configuration of section 4.1 is adopted here. Highly damped material with a loss factor of 0·3 is used for this isolator so that the overall frequency-dependent characteristics are observed without the influence of

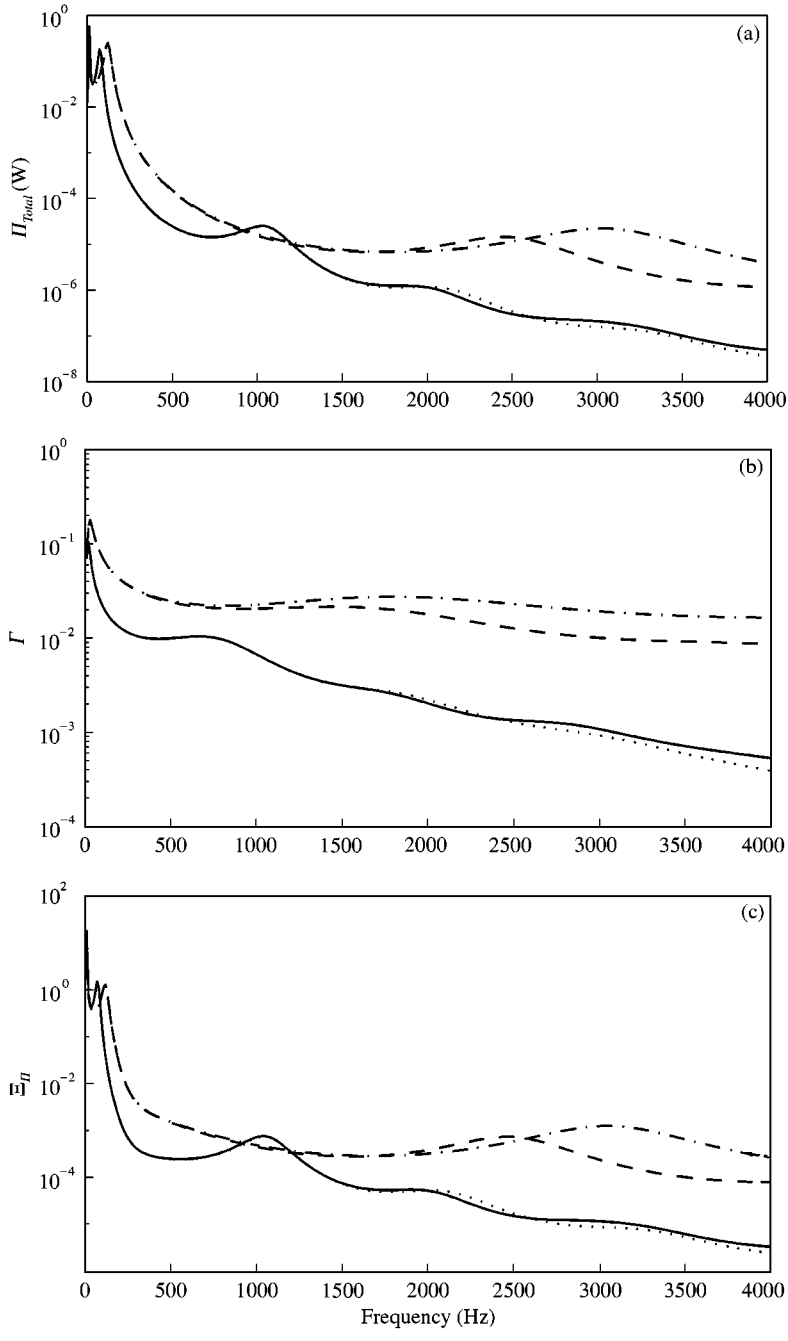

Figure 4. Effect of shear deformation and rotary inertia of an isolator on vibration isolation measures with an infinite beam receiver given a moment excitation. (a) Total transmitted vibration power Π_{Total}; (b) efficiency Γ for total transmitted vibration power; (c) effectiveness Ξ_{Π} for total transmitted vibration power: ——, Timoshenko beam isolator; ·····, Euler beam isolator with shear deformation; ------, Euler beam isolator with rotatory inertia; – – – – –, Euler beam isolator.

isolator resonances. Results for Γ are shown in Figure 6(a) for a variation in G values for an isolator when a harmonic moment is applied to the mass center of a rigid body source. It is observed in Figure 6(a) that Γ rises due to an increase in G as the frequency increases. Next,

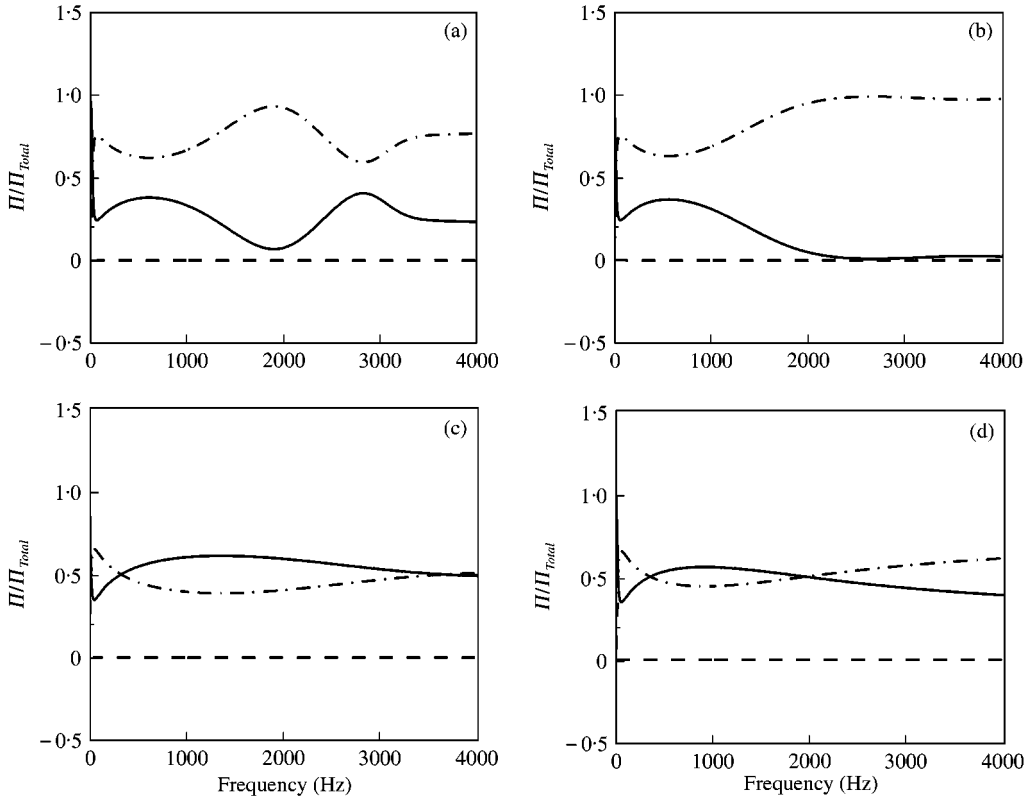

Figure 5. Normalized components of the total power transmitted to the infinite beam given a moment excitation. (a) Timoshenko beam isolator; (b) Euler beam isolator with shear deformation; (c) Euler beam isolator rotary inertia; (d) Euler beam isolator: - - - - -, axial (y); ——, rotational (θ); – – – – –, lateral (x).

Γ is shown in Figure 6(b) when the isolator is modelled by a Euler beam. Similar to Figure 6(a), Γ rises as G increases. However, observe that the spectra of Figure 6(b) tend to stay almost flat as the frequency increases but those of Figure 6(a) for the Timoshenko beam model decrease as the frequency increases. This is because the rotational power component is dominant for the system with a Euler beam isolator and the real part of the rotational mobility for receiver beam increases with frequency. The power efficiency is also shown in Figure 6(c) when a harmonic force (f_y) is applied to the mass center of a source. In this case, only axial stiffness of the mount affects vibration power transmission. Like the moment application case, Γ grows with G as the frequency increases. Also, note that the Γ spectra of Figure 6(c) for the axial power transmission are closer to unity at low frequencies unlike those of Figures 6(a, b) for the flexural power transmission. Normalized power components with respect to the total actual power transmitted to the receiver beam are also shown in Figures 7(a–c) for the shear modulus variation along with absolute power components in Figure 7(d) with the baseline G value. As discussed previously, axial and coupling power components do not exist in this case and therefore the sum of the normalized lateral (shear direction of mount) and rotational power components is equal to unity. Overall, the lateral power component is larger than the rotational component. It is shown in Figures 7(b, d) that the lateral component dominates.

Commonly, designers specify mounts in terms of lumped stiffness elements rather than continuous system properties. Therefore, the following static stiffness ratios (α) are defined.

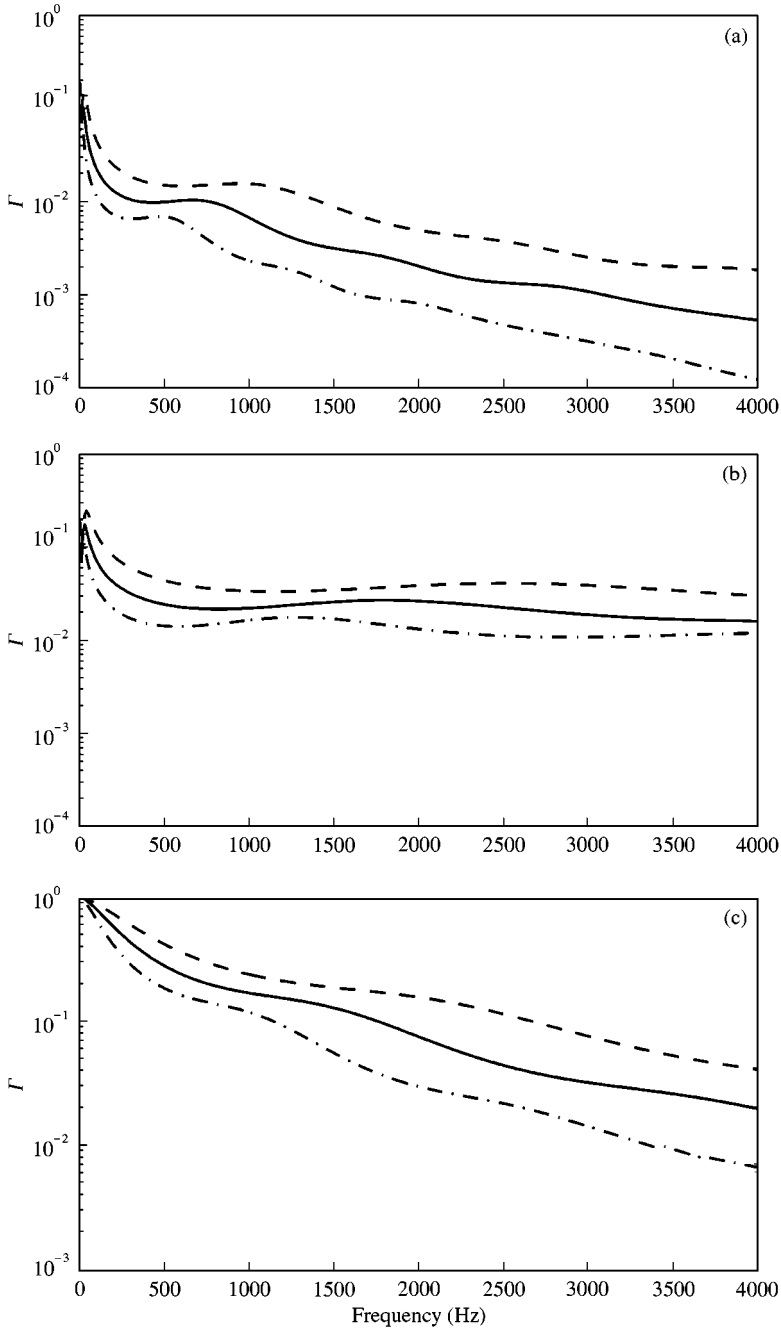

Figure 6. Effect of shear modulus G of an isolator beam on efficiency (Γ) with an infinite beam receiver. (a) For a Timoshenko beam isolator model; (b) for an Euler beam isolator model given a moment excitation; (c) given a force excitation f_y: – – – – –, 0·5G; ——, G; – · – · –, 2G.

Here, each ratio is normalized with respect to the axial component:

$$\alpha_{xy} = \frac{K_{Sx}}{K_{Sy}}, \qquad \alpha_{cy} = \frac{K_{Sc}}{K_{Sy}}, \qquad \alpha_{\theta y} = \frac{K_{S\theta}}{K_{Sy}}, \tag{36a–c}$$

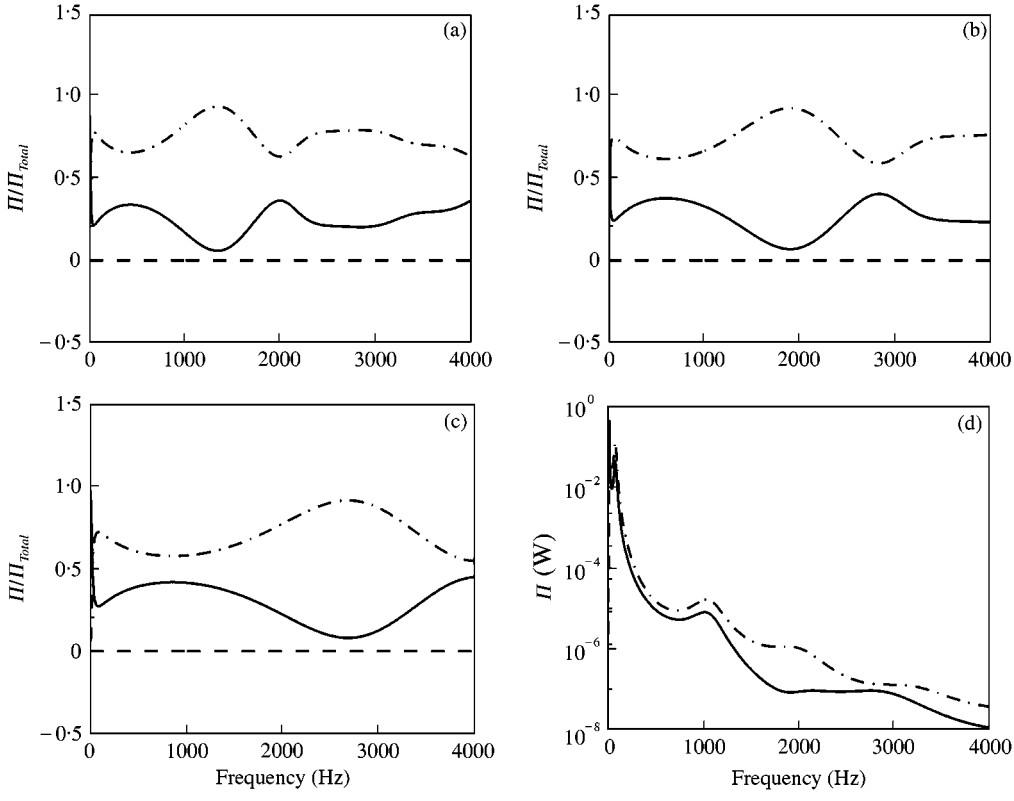

Figure 7. Vibration transmitted to the infinite beam given a moment excitation. (a) Normalized power for 0·5G; (b) normalized power for G; (c) normalized power for 2G; (d) power in W for G: - - - - -, axial (y); ——, rotational (θ); – – – – –, lateral (x).

where α_{xy}, α_{cy} and $\alpha_{\theta y}$ are the ratios of shear, coupling and rotational stiffness components to the axial stiffness respectively. For a cylindrical isolator, the static flexural stiffnesses of equation (34) are represented in terms of the static axial stiffness (K_{Sy}) as follows by using equations (34) and (35):

$$\mathbf{K}_{ST} = \frac{\kappa K_{Sy}^2}{4(1+\nu)[\pi G\kappa L + 3K_{Sy}]} \begin{bmatrix} -6 & -3L \\ 3L & L^2[1 - 3K_{Sy}/2\pi\kappa LG] \end{bmatrix}. \tag{37}$$

Key parameters include the slenderness ratio (S/L), material properties (G and ν) and K_{Sy}. In this case, it is observed from equation (37) that the flexural stiffnesses change when L is varied proportionally to S, unlike the K_{Sy} value. Note that this behavior is also true for the Euler beam case. Note that α_{xy} decreases but both α_{cy} and $\alpha_{\theta y}$ increase as the L or S value increases, while holding S/L, G and ν. The effects of α_{xy} on efficiency (Γ) are examined in Figure 8 for the case when L proportionally varies with S. Figure 8(a) shows that Γ increases as α_{xy} increases at higher frequencies when a harmonic moment is applied at the mass center of a source. Similar to the previous case, Γ with an isolator modelled by a Euler beam is shown in Figure 8(b). Unlike the system with a Timoshenko beam isolator, Γ decreases as α_{xy} increases at higher frequencies. Note that the minimum value of α_{xy} produces the best vibration isolation (hence the lowest Γ) for a system with a Timoshenko beam isolator as shown in Figure 8(a). Therefore, shear deformation and rotary inertia play important roles

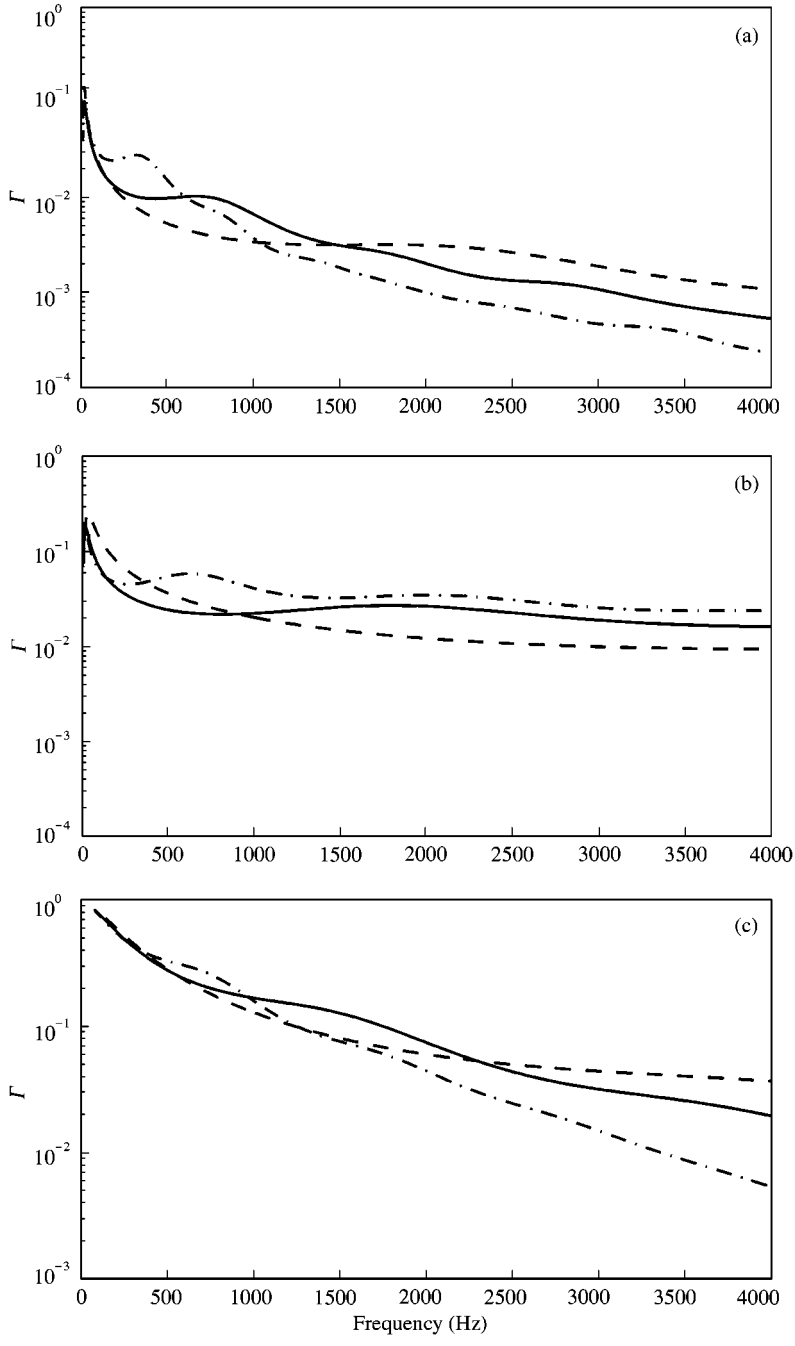

Figure 8. Effect of α_{xy} (ratio of shear to axial components of static stiffness) of an isolator beam on efficiency (Γ) with an infinite beam receiver. (a) For a Timoshenko beam isolator model given a moment excitation; (b) for a Euler beam isolator model given a moment excitation; (c) given a force excitation f_y: – – – – –, $0{\cdot}7\alpha_{xy}$; ——, α_{xy}; – – – – –, $1{\cdot}3\alpha_{xy}$.

in influencing isolation measures. The Γ spectra are shown in Figure 8(c) when a harmonic force (f_y) is applied to a source. Note that K_{Sy} is the only component that affects the power transmission and K_{Sy} is unchanged as α_{xy} is varied in this case. As expected, Γ remains

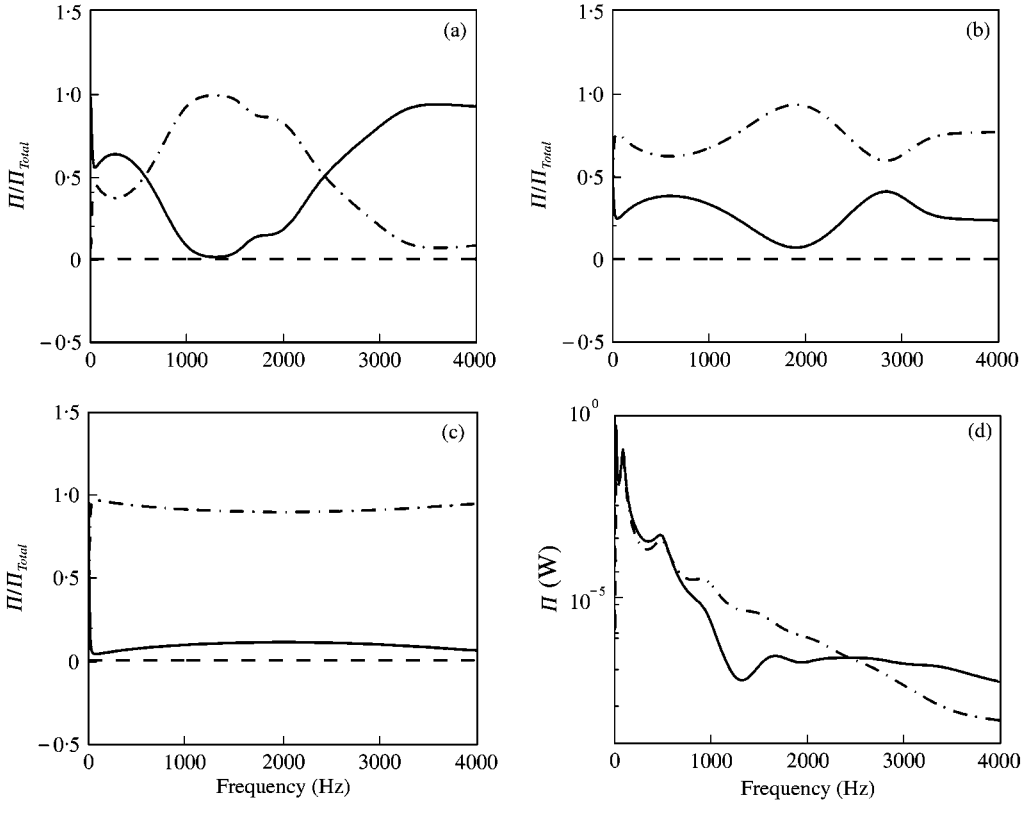

Figure 9. Vibration transmitted to the infinite beam given a moment excitation. (a) Normalized power for $0{\cdot}7\alpha_{xy}$; (b) normalized power for α_{xy}; (c) normalized power for $1{\cdot}3\alpha_{xy}$; (d) power in W for $0{\cdot}7\alpha_{xy}$: - - - -, axial (y); ——, rotational (θ); – – – – –, lateral (x).

unchanged for the α_{xy} variations at lower frequencies. However, it is observed in Figure 8(c) that Γ increases as α_{xy} increases at higher frequencies. Similar to the previous case, vibration power components are calculated in Figure 9. The dominance of lateral and rotational power components changes at a certain frequency for the lowest α_{xy} value as shown in Figures 9(a, d) for both normalized and absolute powers respectively. Observe that for the lowest α_{xy} value case the rotational power component is dominant at lower frequencies and continues to dominate up to the mid-frequency regime where the lateral component is important. However, the lateral component becomes more significant when α_{xy} is increased and the rotational component is negligible for the highest α_{xy} case. Next, the effects of the isolator shape on isolation measures are examined. The shape factor (β) of an isolator is defined as $\beta = L/d$. Note that an increase in β reduces the static flexural and axial stiffnesses as seen from equations (34) and (35). Results are shown in Figure 10. The Γ value decreases at higher frequencies as β increases for both the Timoshenko and Euler beam isolator models when a moment is applied. Similar to the moment excitation case, Γ decreases at higher frequencies as β increases for a force (f_y) excitation case as shown in Figure 10(c). Normalized and absolute vibration power components are also shown in Figure 11 for the lowest β case. Like the previous cases, the lateral component is larger than the rotational component over all the frequencies. However, the rotational component becomes more important at lower and higher frequencies as β is increased.

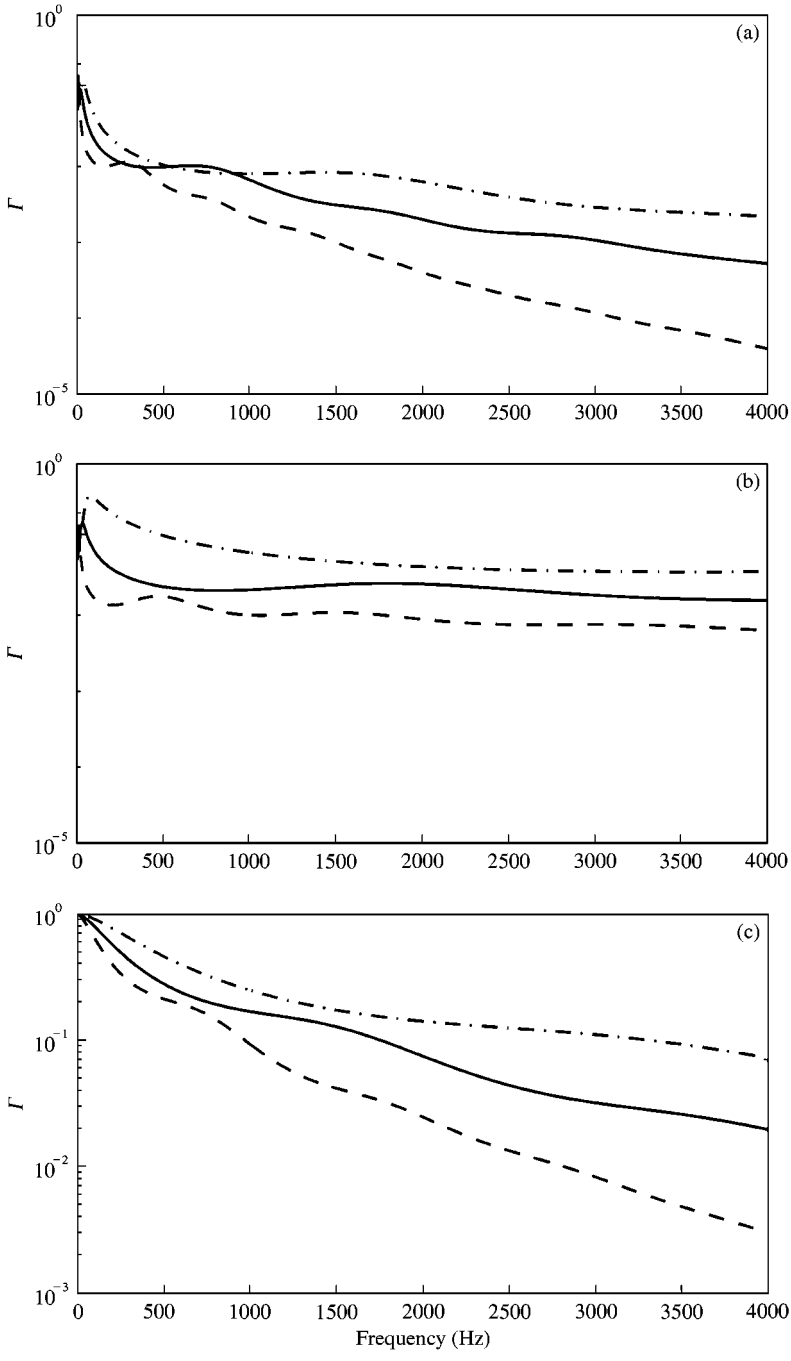

Figure 10. Effect of isolator shape factor β on efficiency (Γ) with an infinite beam receiver. (a) For a Timoshenko beam isolator model given a moment excitation; (b) for a Euler beam isolator model given a moment excitation; (c) given a force excitation f_y: – – – – –, 0·5β; ——, β; – – – –, 2β.

5. VIBRATION POWER TRANSMITTED TO A FINITE BEAM RECEIVER

A finite beam receiver (with clamped ends) is employed to examine the vibration transmission through the isolator for a system of Figure 1(a). Similar to the system with an

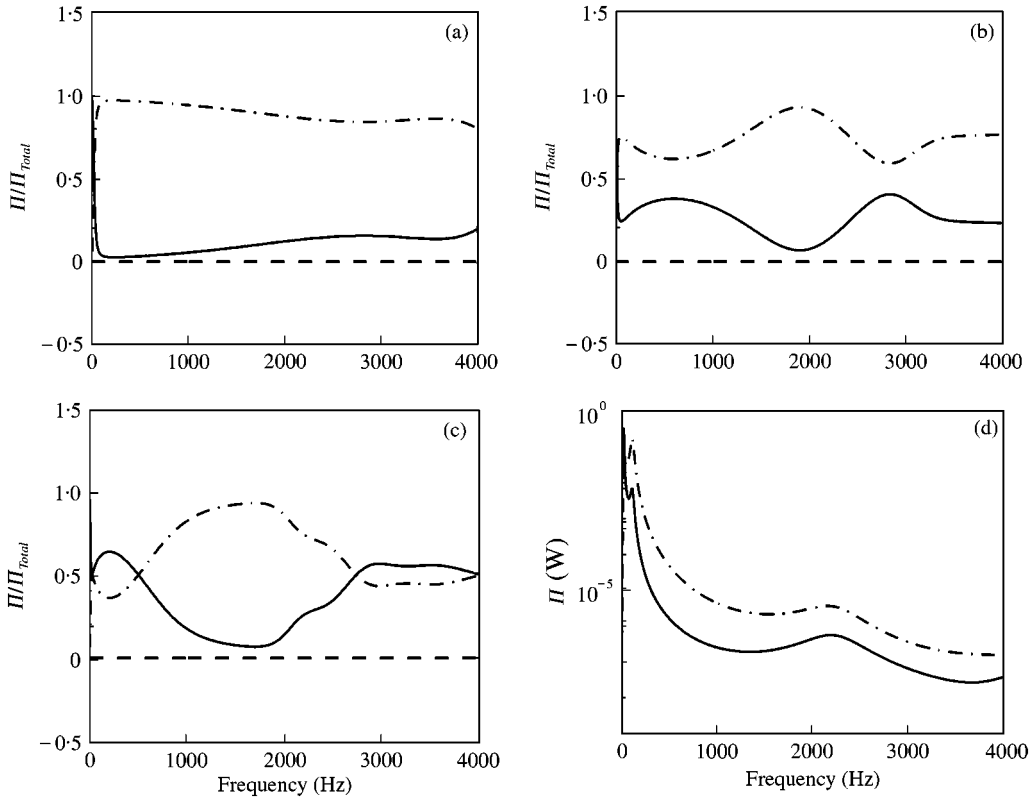

Figure 11. Vibration transmitted to the infinite beam given a moment excitation. (a) Normalized power for $0{\cdot}5\beta$; (b) normalized power for β; (c) normalized power for 2β; (d) power in W for $0{\cdot}5\beta$: - - - - -, axial (y); ——, rotational (θ); – – – – – –, lateral (x).

infinite beam receiver, the Timoshenko beam model and its subsets represent flexural motion of an isolator along with the wave equation for longitudinal motion. Harmonic responses for axial (x) and flexural (y) motions of the receiver beam are, respectively, as follows using the notations of section 4.1:

$$\bar{X}_{RL}(x,t) = X_{RL}(x)\,e^{j\omega t} = [A_{RLx}e^{-jk_{RL}x} + B_{RLx}e^{jk_{RL}x}]\,e^{j\omega t}, \tag{38a}$$

$$\bar{X}_{RR}(x,t) = X_{RR}(x)\,e^{j\omega t} = [A_{RRx}e^{-jk_{RL}x} + B_{RRx}e^{jk_{RL}x}]\,e^{j\omega t}, \tag{38b}$$

$$\bar{Y}_{RL}(x,t) = Y_{RL}(x)\,e^{j\omega t} = \{A_{RLy}e^{-j[k_{RB}x]} + B_{RLy}e^{-[k_{RB}x]} + C_{RLy}e^{j[k_{RB}x]} + D_{RLy}e^{[k_{RB}x]}\}\,e^{j\omega t}, \tag{38c}$$

$$\bar{Y}_{RR}(x,t) = Y_{RR}(x)\,e^{j\omega t} = \{A_{RRy}e^{-j[k_{RB}x]} + B_{RRy}e^{-[k_{RB}x]} + C_{RRy}e^{j[k_{RB}x]} + D_{RRy}e^{[k_{RB}x]}\}\,e^{j\omega t}. \tag{38d}$$

The harmonic responses for the isolator are still given by equations (22a, b). The arbitrary constants of the harmonic responses are obtained by solving the following governing equations in addition to equations (24a–l), where L_R is the total length of the receiver beam and L_{RI} is the length between one clamped end and the junction of receiver and isolator:

$$X_{RL}(-L_{RI}) = 0, \qquad X_{RR}(L_R - L_{RI}) = 0, \tag{39a, b}$$

$$Y_{RL}(-L_{RI}) = 0, \qquad Y_{RR}(L_R - L_{RI}) = 0, \tag{39c, d}$$

$$\frac{\mathrm{d}Y_{RL}(-L_{RI})}{\mathrm{d}x} = 0, \qquad \frac{\mathrm{d}Y_{RR}(L_R - L_{RI})}{\mathrm{d}x} = 0. \tag{39e, f}$$

Finally, Π_{Total}, Γ and Ξ are obtained by using equations (25–28) and the resulting harmonic responses, like the infinite beam receiver calculation. An isolator connected to a rigid body source at one end is assumed to be located off-center ($L_{RI} = 3L_R/4$) of the receiver beam in order to incorporate the effect of coupling mobility of the receiver beam. Note that such a coupling mobility does not exist for both centrally driven beam (with both ends clamped) and an infinite beam.

Figure 12 shows the Π_{Total}, Γ and Ξ for a system with various Timoshenko beam models. Results are given in terms of 1/3 octave band center frequencies from 20 to 4000 Hz and only the mean values within each bandwidth are plotted in Figure 12 and similarly in Figures 13–15. Similar to the system with an infinite beam receiver, the Euler beam isolator with shear deformation well represents the Timoshenko beam model except for the frequencies around 2·5 kHz. Further, three isolation measures for the Euler beam isolator with rotary inertia are similar to those with the Euler beam isolator at frequencies less than ω_T. But discrepancies between the Euler beam isolator models that include or exclude rotary inertia are pronounced as the frequency increases. However, it is observed from Figure 12 that the Euler beam isolator models without shear deformation show large deviations from those with shear deformation. The aforementioned behavior is analogous to the results observed for the infinite beam receiver. The effects of G of a Timoshenko beam isolator on Γ are shown in Figure 13(a) when a moment is applied at a source. Like the infinite beam receiver case, Γ increases especially at higher frequencies as G of an isolator increases. However, the deviation from the aforementioned behavior is observed at certain frequencies (around 2 kHz) due to the coupling mobility and resonances of the receiver beam. Figure 13(b) shows the Γ spectra with the Euler beam isolator for a moment excitation case. Again, Γ rises with G, but the increases in Γ are not as much as those with the Timoshenko beam isolator. Like the system with an infinite beam receiver, Γ f the isolator in Figure 13(b) grows as the frequency increases. But Γ of the Timoshenko beam isolator shows the relatively flat spectra over the frequencies as shown in Figure 13(a). When a force f_y is applied to a source, Γ increases as G increases as shown in Figure 13(c). Unlike the case of an infinite beam receiver, Γ is not closer to unity at low frequencies.

Next, the effect of α_{xy} is examined while holding the slenderness and material properties of the mount. Results are shown in Figure 14 for a moment excitation case. Similar to the infinite beam receiver case, Γ increases at higher frequencies as α_{xy} of the Timoshenko beam isolator increases as shown in Figure 14(a). However, the differences in Γ between the higher α_{xy} values are not significant for the Euler beam isolator as shown in Figure 14(b). This observation implies that the α_{xy} influences the shear deformation effect of an isolator. Despite the small differences, Figure 14(b) shows that Γ decreases at higher frequencies as α_{xy} increases for the Euler beam isolator case, like the system with an infinite beam receiver. In addition, Γ is shown in Figure 14(c) when a force f_y is applied and observe that Γ increases at higher frequencies as α_{xy} increases like the moment excitation case even though the static axial stiffness (K_{Sx}) plays a major role in this force excitation case; K_{Sx} remains unchanged for all α_{xy} variations. Note that Γ remains unchanged up to a certain frequency (around 800 Hz in this case) as α_{xy} is varied, as shown in Figure 14(c). Finally, the effects of β on Γ are examined in Figure 15. Similar to the infinite beam receiver case, an increase in β decreases Γ for both moment and force excitation cases.

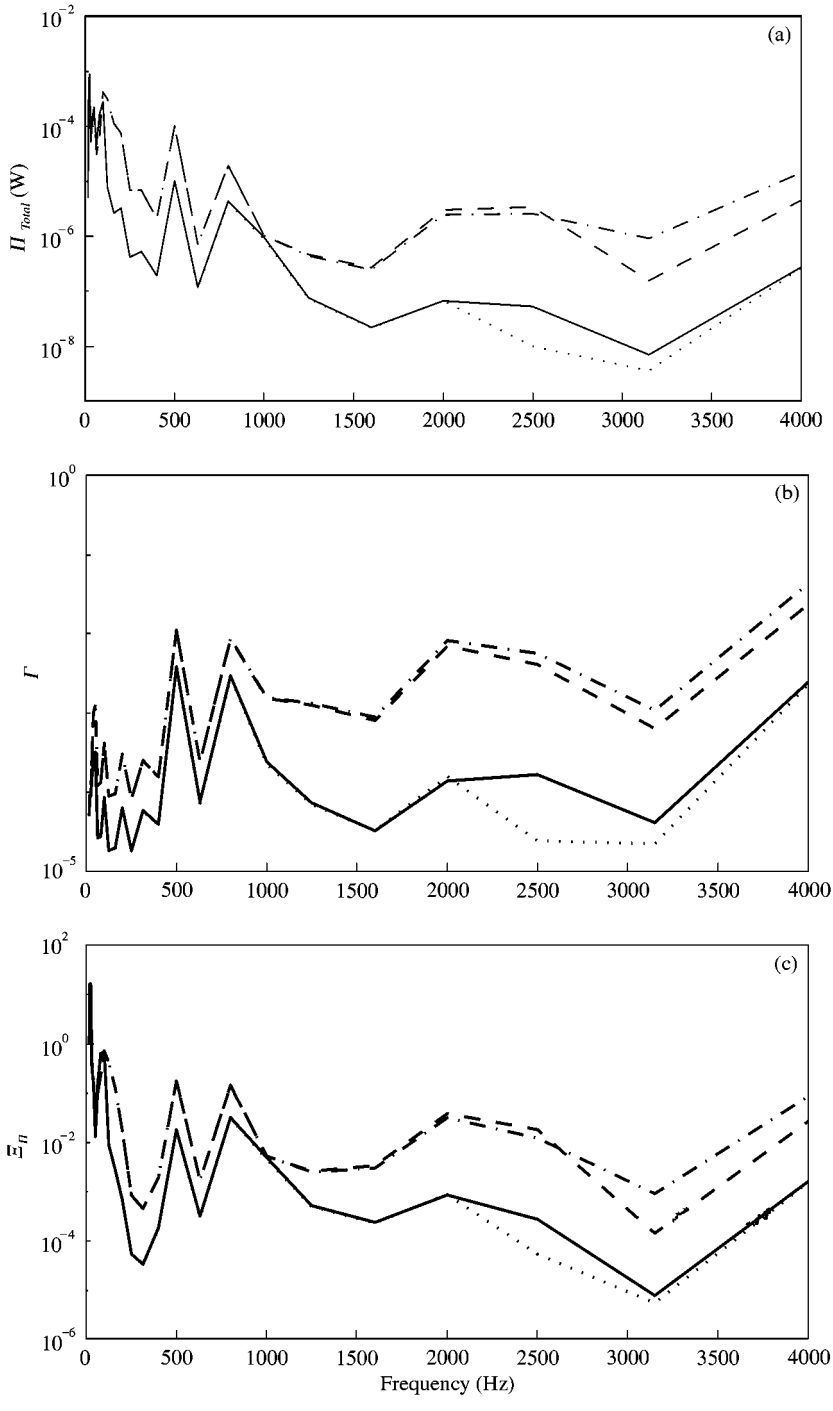

Figure 12. Effect of shear deformation and rotary inertia of an isolator on vibration isolation measures with a finite beam receiver given a moment excitation. (a) Total transmitted vibration power Π_{Total}; (b) efficiency Γ for total transmitted vibration power; (c) effectiveness Ξ_{Π} for total transmitted vibration power: ——, Timoshenko beam isolator; ·····, Euler beam isolator with shear deformation; - - - - -, Euler beam isolator with rotatory inertia; – – – – –, Euler beam isolator. Results are given in terms of 1/3 octave band center frequencies from 20 to 4000 Hz and only the mean values within each bandwidth are plotted here and in Figures 13–15.

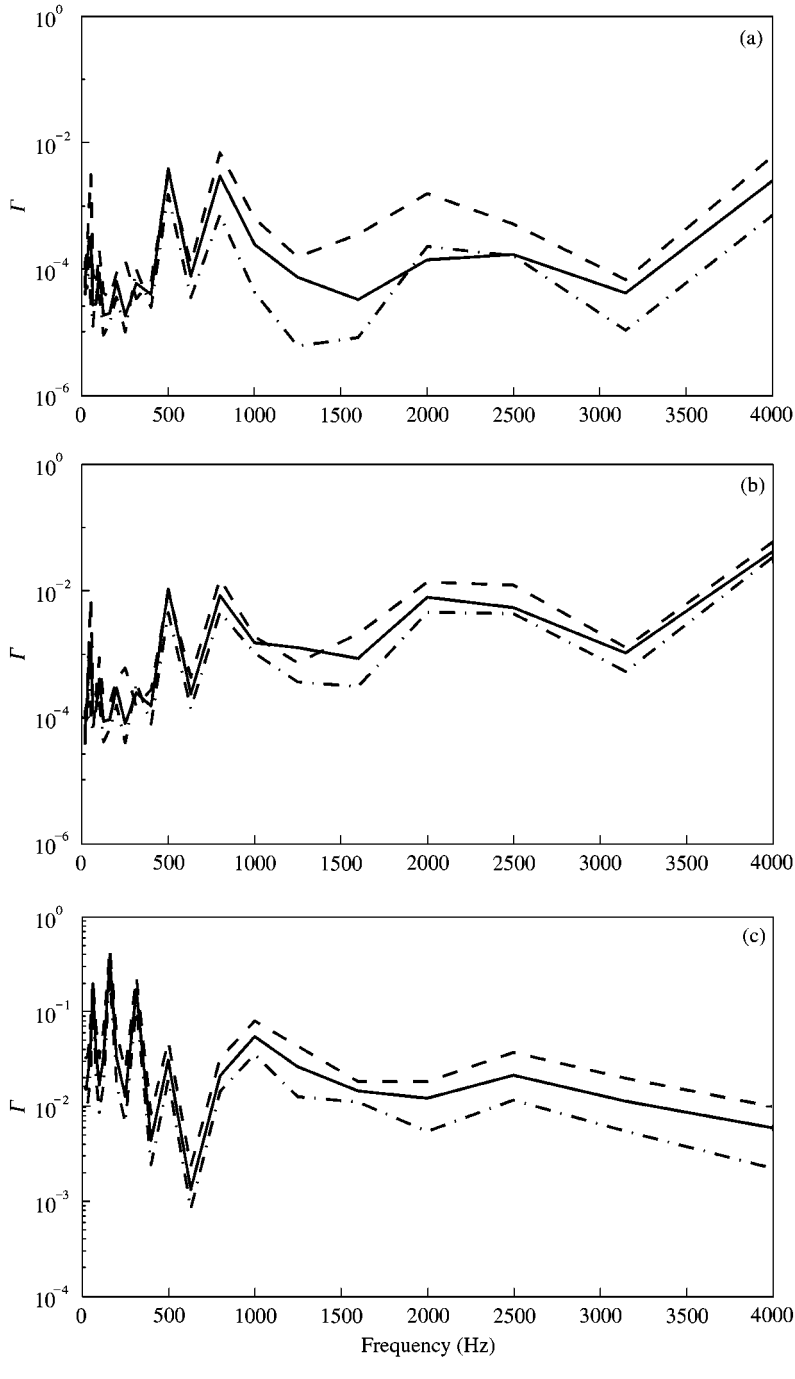

Figure 13. Effect of isolator G on efficiency (Γ) with a finite beam receiver. (a) For a Timoshenko beam isolator model given a moment excitation; (b) for a Euler beam isolator model given a moment excitation; (c) given a force excitation f_y: – – – – –, 0·5G; ——, G; - - - - -, 2G.

6. CONCLUSION

The chief contribution of this paper is the application of continuous system theory to an elastomeric isolator and the examination of associated flexural and longitudinal motions of

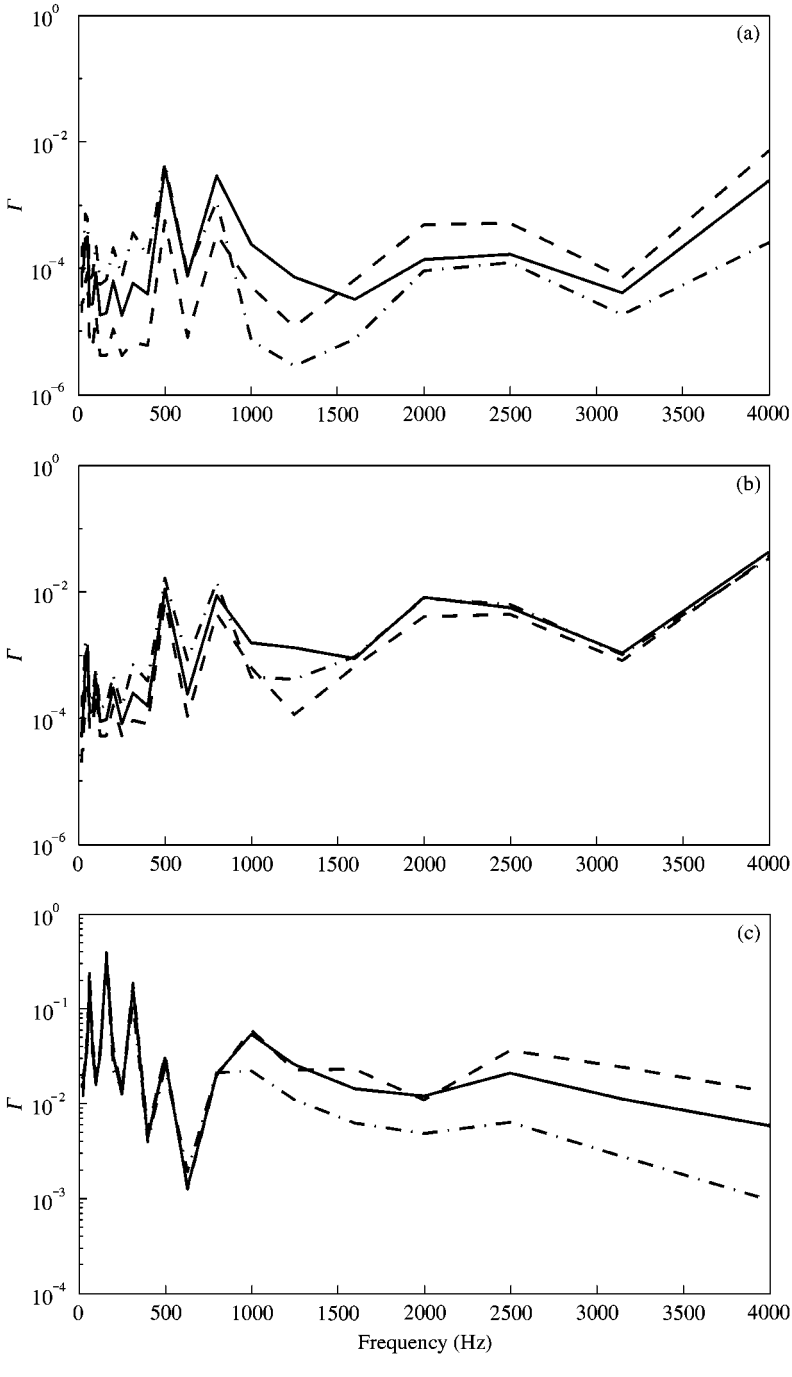

Figure 14. Effect of isolator α_{xy} on efficiency (Γ) with a finite beam receiver. (a) For a Timoshenko beam isolator model given a moment excitation; (b) for a Euler beam isolator model given a moment excitation; (c) given a force excitation f_y: – – – – –, $0{\cdot}3\alpha_{xy}$; ——, α_{xy}; – – – – –, $1{\cdot}3\alpha_{xy}$.

the source–path–receiver system. Two different frequency response characteristics of an elastomeric isolator are predicted by the Timoshenko beam theory. The second type solution, that has been previously believed to occur at extremely high frequencies (say

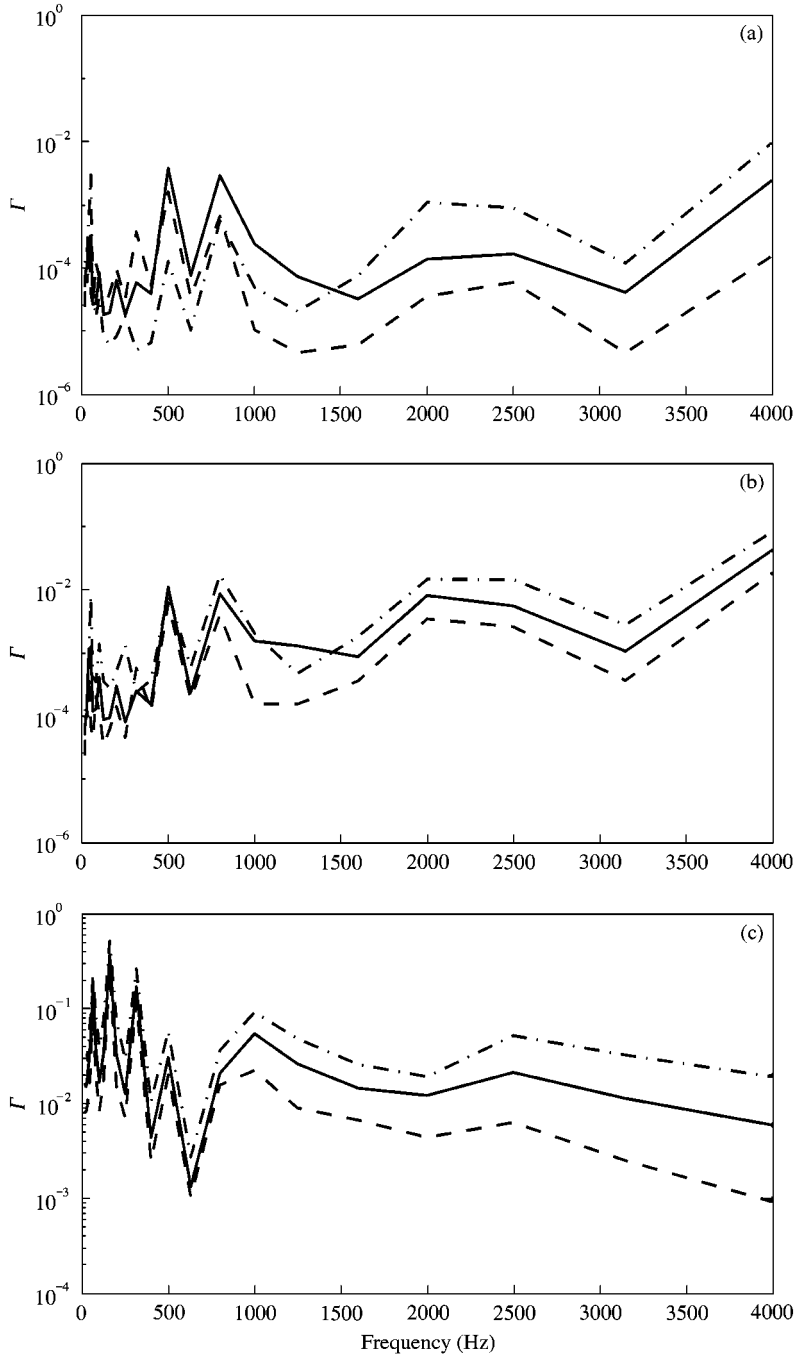

Figure 15. Effect of isolator shape factor β on efficiency (Γ) with a finite beam receiver. (a) For a Timoshenko beam isolator model given a moment excitation; (b) for a Euler beam isolator model given a moment excitation; (c) given a force excitation f_y: – – – – –, 0·5β; ——, β; – – – –, 2β.

around 80 kHz) for metallic structures and therefore not of interest in structural dynamics, takes place at relatively low frequencies (say around 1·5 kHz) for a rubber-like material. The behavior of a typical vibration isolation system has been examined using the power

transmitted to an infinite beam or a finite beam receiver, when excited by a harmonic moment or force at the source. The continuous system analysis clearly shows that the shear deformation and rotary inertia must be considered in order to properly describe the transmission of flexural motions at higher frequencies. In particular, the shear deformation effect is found to be more pronounced than the role of the rotary inertia, as evaluated by the power-based vibration isolation measures at higher frequencies. Parametric study of isolator parameters on the transmission measures has been conducted using the Timoshenko beam isolator model and an infinite beam receiver. Material and geometric parameters of an isolator have been examined along with the static stiffness ratios (between K_{Sy}, K_{Sx} and $K_{S\theta}$ components). The vibration power efficiency, effectiveness and power transmitted to an infinite beam structure increase with frequency as the isolator shear modulus increases. Resulting characteristics for a system with a finite beam receiver confirm the trends.

Future work is required to quantify the vibration source in terms of power transmission. Future analysis must also incorporate the effect of compliant sources for a single or a multi-isolator system on the vibration power transmission. Further, an experimental investigation is needed to confirm the phenomena identified in this article. Proper interpretation of various vibration isolation measures for a multi-dimensional system, such as power efficiency and effectiveness, must also be sought over a broad range of frequencies. Finally, non-linear effects of an isolator should be examined.

ACKNOWLEDGMENTS

The General Motors Corporation (Noise and Vibration Center) and the Goodyear Tire and Rubber Company (Transportation Molded Products) are gratefully acknowledged for supporting this research.

REFERENCES

1. T. JEONG and R. SINGH 2001 *Journal of Sound and Vibration* **245**, 385–415. Inclusion of measured frequency- and amplitude-dependent mount properties in vehicle or machinery models.
2. H. G. D. GOYDER and R. G. WHITE 1980 *Journal of Sound and Vibration* **68**, 97–117. Vibrational power flow from machines into built-up structures, part III: power flow through isolation systems.
3. J. I. SOLIMAN and M. G. HALLAM 1968 *Journal of Sound and Vibration* **8**, 329–351. Vibration isolation between non-rigid machines and non-rigid foundations.
4. J. C. SNOWDON 1968 *Vibration and Shock in Damped Mechanical Systems*. New York: John Wiley & Sons, Inc.
5. M. A. SANDERSON 1996 *Journal of Sound and Vibration* **198**, 171–191. Vibration isolation: moments and rotations included.
6. W. L. LI and P. LAVRICH 1999 *Journal of Sound and Vibration* **224**, 757–774. Prediction of power flows through machine vibration isolators.
7. J. PAN, J. PAN and C. H. HANSEN 1992 *Journal of the Acoustical Society of America* **92**, 895–907. Total power flow from a vibrating rigid body to a thin panel through multiple elastic mounts.
8. E. E. UNGAR and C. W. DIETRICH 1966 *Journal of Sound and Vibration* **4**, 224–241. High-frequency vibration isolation.
9. L. L. BERANEK 1988 *Noise and Vibration Control*. Washington, DC: Institute of Noise Control Engineering.
10. P. GARDONIO, S. J. ELLIOTT and R. J. PINNINGTON 1997 *Journal of Sound and Vibration* **207**, 61–93. Active isolation of structural vibration on a multiple-degree-of-freedom system, part I: the dynamics of the system.
11. P. GARDONIO and S. J. ELLIOTT 2000 *Journal of Sound and Vibration* **237**, 483–511. Passive and active isolation of structural vibration transmission between two plates connected by a set of mounts.

12. S. KIM and R. SINGH 2001 *Journal of Sound and Vibration* **245**, 877–913. Multi-dimensional characterization of vibration isolators over a wide range of frequencies.
13. L. F. NIELSEN, N. J. WISMER and S. GADE 2000 *Sound and Vibration* 20–24. An improved method for estimating the dynamic properties of materials.
14. L. CREMER, M. HECKLE and E. E. UNGAR 1973 *Structure-Borne Sound*: *Structural Vibrations and Sound Radiation at Audio Frequencies*. New York: Springer-Verlag.
15. R. G. DEJONG, G. E. ERMER, C. S. PAYDENKAR and T. M. REMTEMA 1998 *Noise-Con* 98, *Ypsilanti*, *Michigan*, *U.S.A*. High frequency dynamic properties of rubber isolation elements.
16. R. W. TRAILL-NASH and A. R. COLLAR 1953 *Quarterly Journal of Mechanics and Applied Mathematics* **6**, 186–222. The effect of shear flexibility and rotary inertia on the bending vibrations of beams.
17. J. F. DOYLE 1997 *Wave Propagation in Structures*: *Spectral Analysis Using Fast Discrete Fourier Transforms*. New York: Springer-Verlag.
18. S. GOPALAKRISHNAN, M. MARTIN and J. F. DOYLE 1992 *Journal of Sound and Vibration* **158**, 11–24. A matrix methodology for spectral analysis of wave propagation in multiple connected Timoshenko beams.
19. R. E. D. BISHOP and D. C. JOHNSON 1960 *The Mechanics of Vibration*. Cambridge: Cambridge University Press.

APPENDIX A: NOMENCLATURE

A, B, C, D	arbitrary constants
b	width
d	diameter
E	Young's modulus
f	force amplitude
F	axial force
G	shear modulus
h	distance between rigid body center and mount interface
I_S	area moment of inertia
I_m	mass moment of inertia
j	$\sqrt{-1}$
k	wave number
K	stiffness
$\mathbf{K}$	stiffness matrix
L	length
m	mass
M	moment
q	moment amplitude
Q	empirical constant for rubber material
r	radius
r_g	radius of gyration
R	variable for root transition
S	area
t	thickness
T	shape factor for rubber material
v	translational velocity
V	shear force
w	load intensity function
w	rotational velocity
X	displacement in x direction
Y	displacement in y direction
x, y, z	Cartesian co-ordinates
α	static stiffness ratio
β	shape factor of isolator (L/d)
Γ	efficiency of vibration power
η	loss factor
θ	rotational displacement

κ	shear constant
λ	root of differential equation
ν	the Poisson ratio
ξ	non-dimensionalized co-ordinate
Ξ	effectiveness of vibration power
Π	vibration power (time-averaged)
ρ	mass density
$\chi, \varepsilon, \mu, \tau, \upsilon$	parameters for Timoshenko beam
ω	frequency, rad/s
ω_T	transition frequency, rad/s

Subscripts

B	bending
c	coupling
E	Euler beam
G	mass center
IN	input
L	axial or longitudinal motion
P	isolator (path)
R	receiver
RI	interfacial location of receiver beam with isolator
RL	left-travelling wave in receiver
RR	right-travelling wave in receiver
S	static
T	Timoshenko beam or transition frequency
Total	sum of power components transmitted to receiver
with	with isolator
without	without isolator
x, y, z	Cartesian co-ordinates
$0, L$	beam locations
θ	rotational

Superscripts

$\sim$	complex valued
*	complex conjugate
$-$	function of time and spatial co-ordinates

Operators

Re	real part